Chapter 5

Interpretation and Visualization of Results

Contents

5.1 Measurement Database

MATSTAB was validated against a large number of measurements in seven reactors situated at three different sites. While the next chapter describes the results of the validation, this chapter explains how MATSTAB differs from other codes, and how this difference may be used to produce new insights.

As a base for these explanations the measurement series conducted in Leibstadt in 1990 (cycle 7)[12] and 1993 [86] are chosen. These measurements were very thoroughly prepared and covered a wide range of operating points. Even more, the detailed post analysis showed regional oscillations in 1990.

The fifth operating point (45% power, 28% core flow) from the 1993 measurement series (see also Section 6.2.3) showed global oscillations and served as reference case for many of the following plots.

5.2 Displaying Three Dimensional Variables

MATSTAB represents the reactor with a detailed nodalization scheme and a respectable number of equations and variables. In consequence, a huge amount of data results from the calculations and must be presented carefully to give some insight.

All calculated parameters and variables may be stored for later investigations. The power distribution is presented as an example because its axial shape has undoubtedly an important influence to the stability of the reactor.

Figure 5.1 shows a normalized power-density distribution of the Leibstadt reactor measured during the stability test in 1993 [86]. The colors represent the axially averaged values. Each color square represents a fuel assembly. The larger squares, containing 4 fuel assemblies are called super cells, or controlled cells, in case a cross shaped control rod is allocated in between. The numbers plotted within a super cell are therefore the percentage of which a control rod is withdrawn from the core (fully withdrawn rods are not indicated).

To add the valuable information contained in the axial shapes, it is possible to select a couple of channels (indicated with X in Figure 5.1) and plot their axial values (Figure 5.2). The four chosen channels show a very different axial power distribution. The fuel assemblies in the center and at the boundaries of the core show a flat distribution.

The assembly in the outer part of the core is clearly bottom peaked while the controlled assembly is top peaked since the control rod enters from the bottom.

Figure 5.3 shows the radially averaged axial power density distribution of all super cells. This Figure gives a good impression of the calculated power density distribution in the core. Any other physical property may be displayed in the same manner. For example, the void content, liquid flow, neutron flux, fuel temperature and so on.

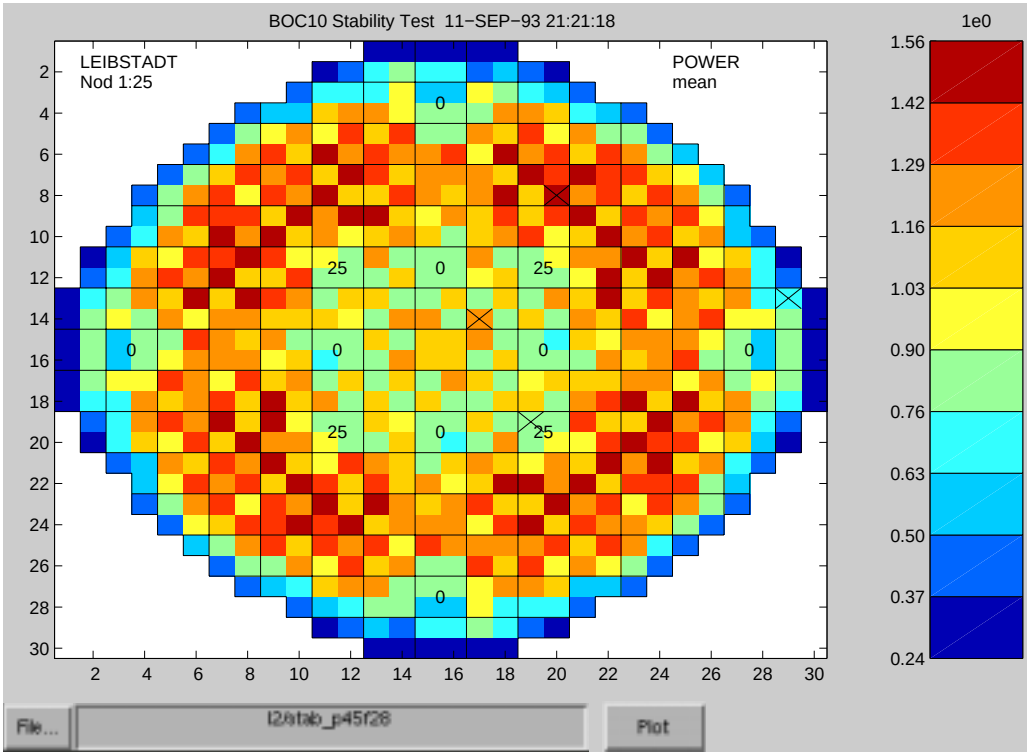

Figure 5.1: Axially Averaged Power Density Distribution of the Leibstadt Reactor

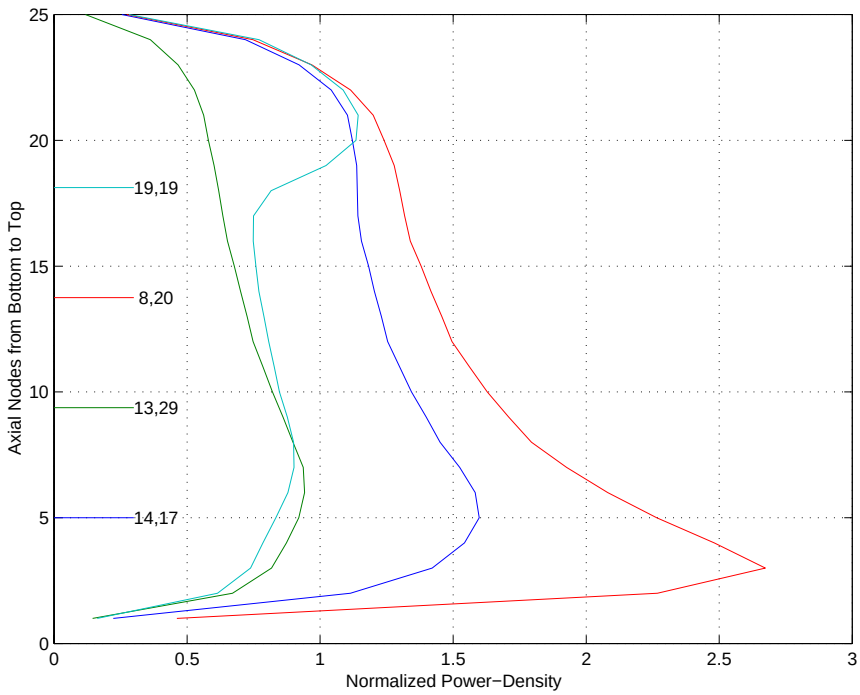

Figure 5.2: Axial Power Shapes in Individual Channels of the Leibstadt Reactor

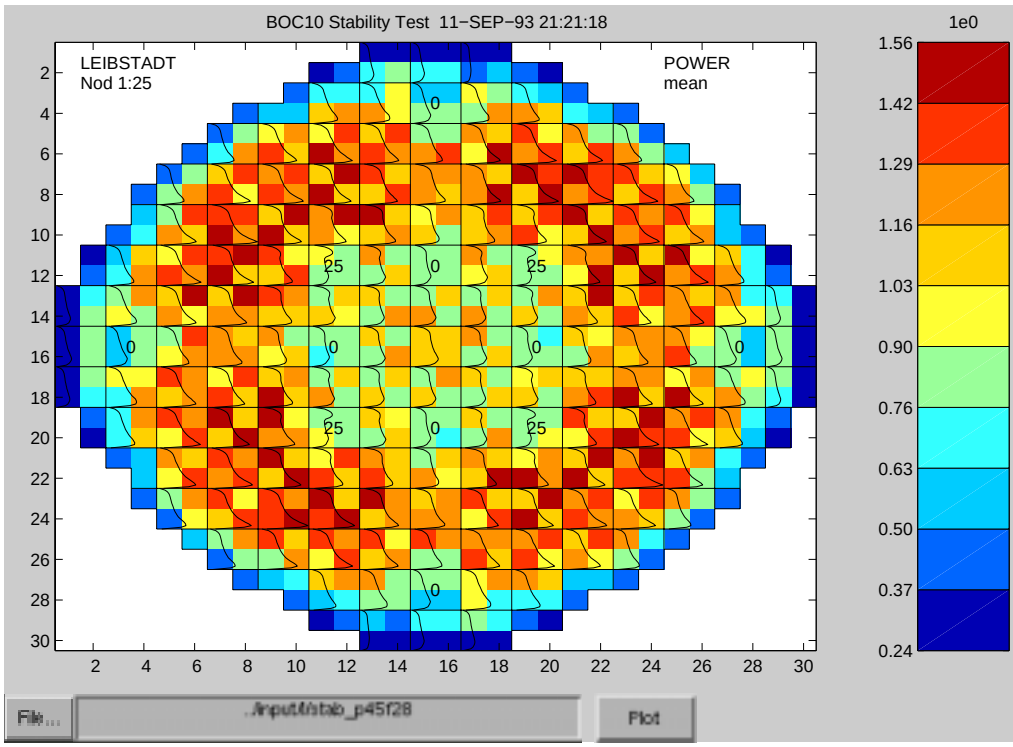

Figure 5.3: Axial Power Shapes in the Leibstadt Reactor

5.3 Eigenvectors

It was stressed several times before that a wealth of information may be gained from an investigation of the left and right eigenvectors of the dominating oscillation modes. The availability of the eigenvectors which come naturally from the calculation of the eigenvalue (see Section 4.3 Equation 4.6), are a major advantage of MATSTAB as will be shown in the following pages.

Equation 2.25 describes the mode j of a chosen variable $\Delta\mathbf{x}_j(\tau)$ in terms of the dominating eigenvalue λ_j, the corresponding left and right eigenvectors $\mathbf{f}_j$ and $\mathbf{e}_j$ and the value at time $\tau = 0$ of the mode considered.

$$\Delta\mathbf{x}_j(\tau) = \mathbf{e}_j e^{\lambda_j \tau}[\mathbf{f}_j^T \Delta\mathbf{x}_j(0)] \tag{2.25}$$

5.3.1 Right Eigenvector

The right eigenvector $\mathbf{e}_j$ describes the relative magnitude and phase of the dominating mode $\Delta\mathbf{x}_j(\tau)$ of the state variable $\mathbf{x}(\tau)$. Since both $e^{\lambda_j\tau}$ and $\mathbf{f}_j^T\Delta\mathbf{x}_j(0)$ are scalars, the shape of the mode $\Delta\mathbf{x}_j(\tau)$ is entirely defined by $\mathbf{e}_j$.

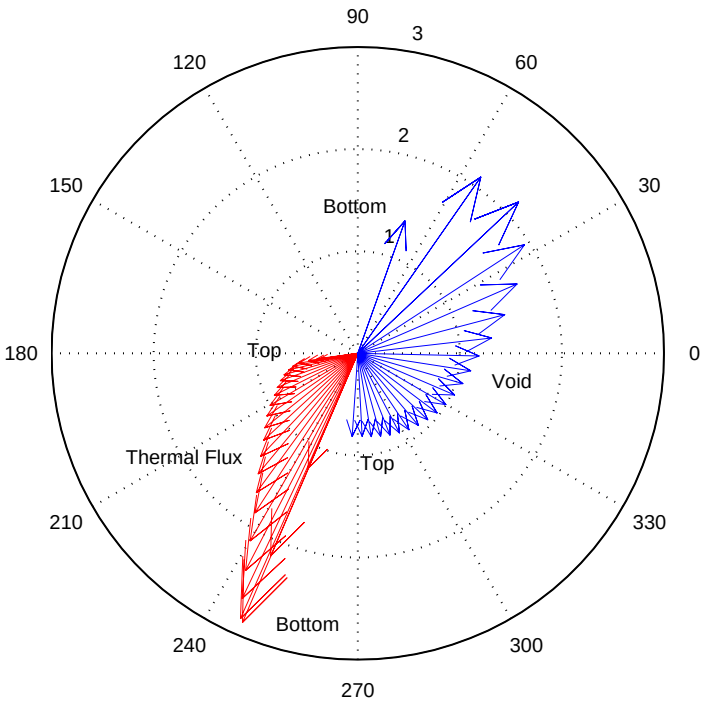

Figure 5.4: Void and Thermal Neutron Flux Phasors in One Channel

The complete eigenvector **e** has a very large number of components, therefore, only its components may be displayed in a reasonable manner.

If just one channel is investigated, it is possible to see the gain as well as the phase shift. The phasors in Figure 5.4 show the phase and gain of the void fraction and of the thermal neutron flux, for all 25 nodes in a specific channel. One can see, that the gain is larger in the bottom part of the reactor and smaller in the upper part. It is also easy to spot, that there is a phase shift of 180 degrees for the void component whereas the phase of the thermal flux component is only shifted by ≈ 60 degrees from bottom to top. The channel was selected randomly and represents the normal situation in a channel. Figure 5.5 shows the absolute value of the eigenvector component that corresponds to the thermal flux.

5.3.2 Left Eigenvector

Equation 2.25 also clarifies the role of the left eigenvector $\mathbf{f}_j$. The left eigenvector $\mathbf{f}_j$ determines how the mode is excited by the initial conditions. Note that if $\Delta\mathbf{x}_j(0) = k * \mathbf{e}_j$ for some scalar k, then only the mode j is excited, $\Delta\mathbf{x}(\tau) = \Delta\mathbf{x}_j(\tau)$, since $\mathbf{F}^{\mathbf{T}}\mathbf{E} = \mathbf{I}$ by definition 2.18.

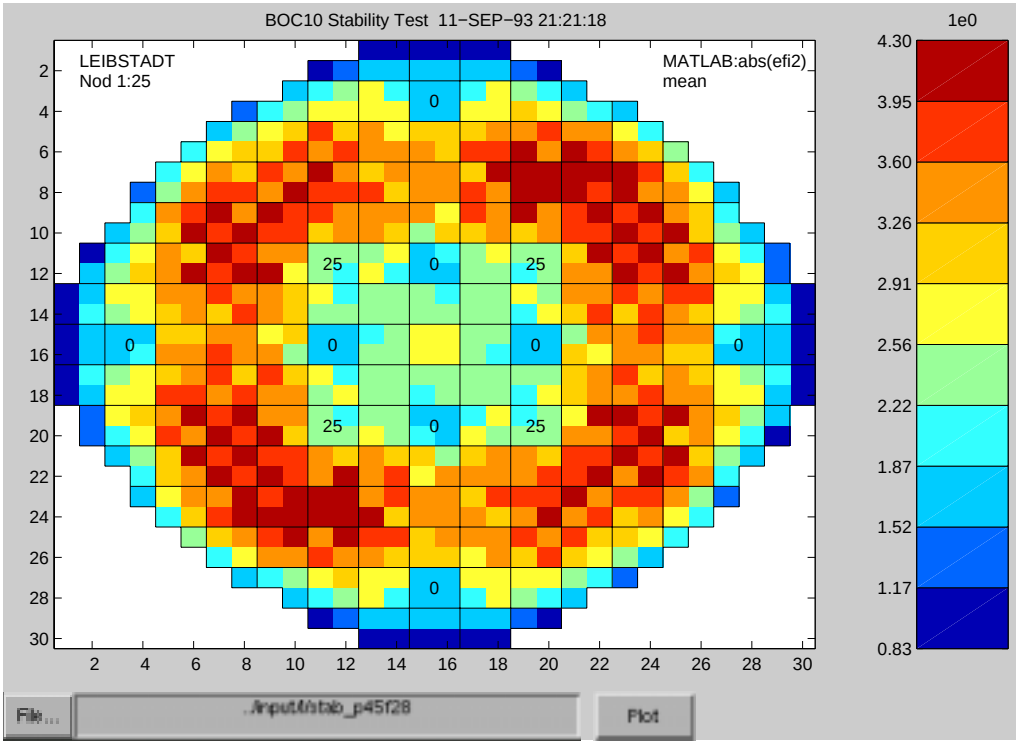

Figure 5.5: Thermal Flux (Absolute Value) of the Right Eigenvector (Axially Averaged)

5.4 The Contributors to the Eigenvalue/Decay Ratio

The real value of the left eigenvector **f** lies in the possibility to broaden the decay ratio concept. The following section outlines a methodology to calculate the contribution of any model component to the eigenvalue/decay ratio and hence to the stability of the system. It is possible to analyze the contribution of any model section, channel, node, equation or parameter to the eigenvalue and hence stability of the system.

The eigenvalue and consequently also the decay ratio, is no longer only one number describing the overall behavior of the coupled system. The number is composed from different components, each of which has its own physical meaning. For example, it is possible to calculate the contribution of each fuel assembly to the eigenvalue or the contribution of a specific equation (e.g. slip) or section (e.g. riser) in the model.

In MATSTAB, the dominating eigenvalue λ is obtained directly during the iterative calculation of the right eigenvector. However, it is instructive to represent the eigenvalue by means of both (left and right) eigenvectors.

Multiplying the basic equation of the generalized eigenvalue problem (Equation 2.15)

$$\mathbf{A}_s\mathbf{e} = \lambda\mathbf{B}\mathbf{e} \tag{2.15}$$

from the left with the left eigenvector, leads to

$$\mathbf{f}^T\mathbf{A}_s\mathbf{e} = \lambda\mathbf{f}^T\mathbf{B}\mathbf{e} \tag{5.1}$$

$$\lambda = \frac{\mathbf{f}^T\mathbf{A}_s\mathbf{e}}{\mathbf{f}^T\mathbf{B}\mathbf{e}} \tag{5.2}$$

$$\lambda = \mathbf{f}^T\mathbf{A}_s\mathbf{e} \tag{5.3}$$

because $\mathbf{f}^T\mathbf{B}\mathbf{e}$=1 due to the scaling of $\mathbf{f}^T$. It is interesting to investigate Equation 5.3 a bit further.

$$\lambda = \mathbf{f}^T\mathbf{A}_s\mathbf{e} \tag{5.4}$$

$$= \sum_{k=1}^{n} f_k \sum_{l=1}^{n} a_{k,l}e_l \tag{5.5}$$

$$= \sum_{k,l} f_k a_{k,l} e_l \tag{5.6}$$

$$\lambda = \begin{bmatrix}1 & \dots & 1\end{bmatrix} \begin{bmatrix} f_1a_{1,1}e_1 & \dots & f_1a_{1,n}e_n \\ \vdots & f_ka_{k,l}e_l & \vdots \\ f_na_{n,1}e_1 & \dots & f_na_{n,n}e_n \end{bmatrix} \begin{bmatrix}1\\ \vdots \\ 1\end{bmatrix} \tag{5.7}$$

The introduced matrix

$$\mathbf{A}_\lambda = \begin{bmatrix} f_1a_{1,1}e_1 & \dots & f_1a_{1,n}e_n \\ \vdots & f_ka_{k,l}e_l & \vdots \\ f_na_{n,1}e_1 & \dots & f_na_{n,n}e_n \end{bmatrix} \tag{5.8}$$

has very interesting properties. The first and most obvious is that the sum of all matrix elements equals the eigenvalue λ.

But furthermore, the entries $f_ka_{k,l}e_l$ of the matrix $\mathbf{A}_\lambda$ represent each a dependency of a certain variable in a certain equation in a certain node. Since the number of these entries is large ($\approx 10^6$) and dependent on the nodalization scheme, it is reasonable to sum up some subsets. For example, one can add all summands within the different model sections; neutronics, thermal-hydraulics or the sections outside the core (steam dome, downcomer, etc.). Since the reactor core is a very interesting section, one should also investigate the contributions of the different fuel channels.

Finally, it is also possible to sum up and analyze the contribution of each model equation (row in the matrix) or each variable (column in the matrix). When summing over a node, a channel or a model section, the contribution of e.g. the void fraction equation differs naturally from the contribution of the void fraction variable. Nevertheless, when summing over the complete model, the contributions of equations and their corresponding variables is the same. The reason lies in the fact that the sum over the row j in the matrix $\mathbf{A}_\lambda$ equals the sum over the column j.

$$\sum_{row\,j} \mathbf{A}_\lambda = \sum_{l=1}^{n} f_j a_{j,l} e_l \tag{5.9}$$

$$= f_j \sum_{l=1}^{n} a_{j,l} e_l \tag{5.10}$$

$$= f_j \mathbf{A}_{s,row\,j} \mathbf{e} \tag{5.11}$$

$$= f_j \lambda e_j \tag{5.12}$$

because **e** is an eigenvector of $\mathbf{A}_s$ and

$$\sum_{column\,j} \mathbf{A}_\lambda = \sum_{k=1}^{n} f_k a_{k,j} e_j \tag{5.13}$$

$$= e_j \sum_{k=1}^{n} f_k a_{k,j} \tag{5.14}$$

$$= e_j \mathbf{f}^T \mathbf{A}_{s,column\,j} \tag{5.15}$$

$$= e_j \lambda f_j \tag{5.16}$$

$$= \sum_{row\,j} \mathbf{A}_\lambda \tag{5.17}$$

The expression $\lambda f_j e_j$ is in principle the same as the expression $f_j e_j$ which is well known from control theory as the participation factor. This property of the matrix $\mathbf{A}_\lambda$ is very interesting for further investigations, but should not mislead to the conclusion that the matrix is symmetric. As stated before, only the sum over the complete model is the same for equations and variables. When summing over nodes, channels, etc. the results differ.

Representation of the Decay Ratio as a Product of Contributing Factors

The sum in Equation 5.6 is easy to translate into a product which leads to the decay ratio. As shown in Chapter 2, the decay ratio can be written as

$$DR = e^{\frac{2\pi\sigma}{\omega}} \tag{2.27}$$

$$= e^{\left(\frac{2\pi}{\omega} \sum_{k,l} real(f_k a_{k,l} e_l)\right)} \tag{5.18}$$

$$= \prod_{k,l} e^{\frac{2\pi}{\omega} real(f_k a_{k,l} e_l)} \tag{5.19}$$

$$\equiv \prod_{k,l} dr_{k,l} \tag{5.20}$$

The representation of the eigenvalue as a sum over different contributions seems to be more natural than this representation of the decay ratio as a product of different contributions.

Especially because unimportant objects are 1 in the product representation, which feels a bit strange when speaking about decay ratios. Therefore, the next few sections only deal with the contributions to the eigenvalue where an unimportant object, as expected, contributes with 0.

5.4.1 Contribution of the Model Sections to the Eigenvalue

The Figure 5.6 shows the contribution of the different model sections (outside of the core, thermal-hydraulics, neutronics, flow distribution model, pumps and system pressure) to the real part of the eigenvalue; i.e. the sum of the section contributions equals the real part of the eigenvalue. The four colored bars represent different operating points from the Leibstadt measurement series conducted in 1993 (see Table 6.6 on page 120). For the most stable case, MATSTAB calculated a decay ratio of 0.42 and for the least stable case 1.02.

Unfortunately, Figure 5.6 does not identify a special section as the driving force of instability. The contributions of all sections diminish in a similar way for less stable operating points. The contributions and therefore also the changes in the thermal-hydraulic and neutronic part dominate, however, the behavior of the reactor. In the second plot of Figure 5.6, the contribution of the thermal-hydraulic and neutronic part of the model are added and represented as the contribution of the core. The combined contribution is negative and, therefore, stabilizing. The stabilizing contribution of the thermal-hydraulics over-compensates the destabilizing contribution of the neutronic part. However, the difference becomes smaller for less stable operating points. In other words, when moving from a stable to a less stable operating point, the contributions decrease, but the reduction in the thermal-hydraulic part is larger than the reduction in the neutronic part, hence, the reactor becomes overall less stable.

Figure 5.7 shows this trend. The dashed region, representing the difference between the thermal-hydraulic and neutronic part, diminishes in the less stable region. The interpretation of the absolute value of the contributions is, however, difficult. There are not enough measurements points available to relate the magnitude of a single contribution to the reactor state.

Since in Forsmark always measures the same operating point during start up, it is not possible to generate the corresponding plots for Forsmark. Therefore, some (numerical) studies for different operating points in different power plants are recommended as future work. The necessary steady-state distribution files need, however, to be prepared by the plant, since POLCA is not generally available.

It remains to observe, that the “decay ratio” and “thermal-hydraulics” lines in Figure 5.7 are roughly parallel. This simple relationship between the decay ratio and the contribution of the thermal-dynamics may very well be a coincidence, since only four operating points are involved, but further investigations when more operating points are available are recommended.

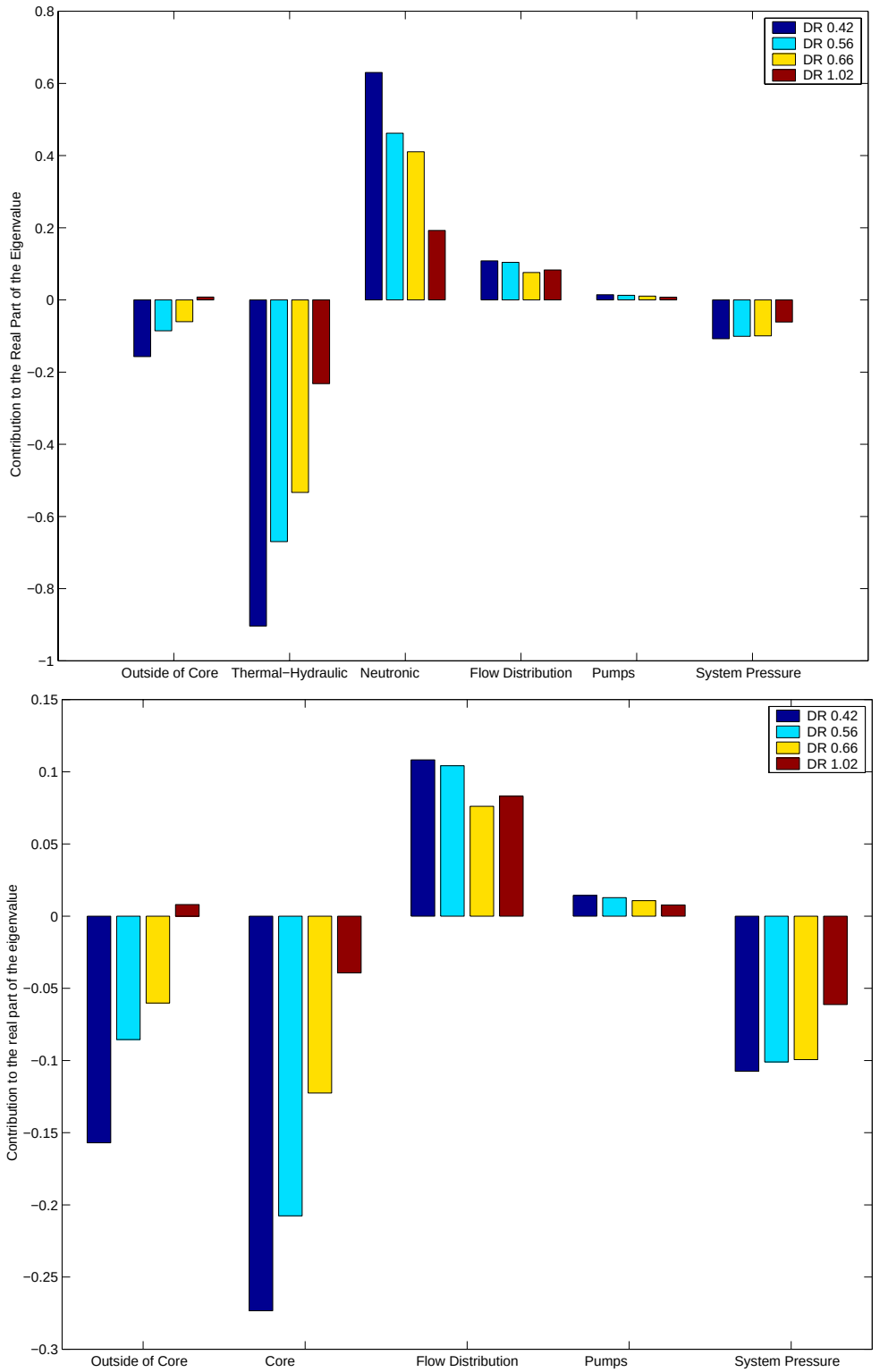

Figure 5.6: Contribution of Each Model Section of the Reactor for Different Operating Points (for 5 and 6 Model Sections)

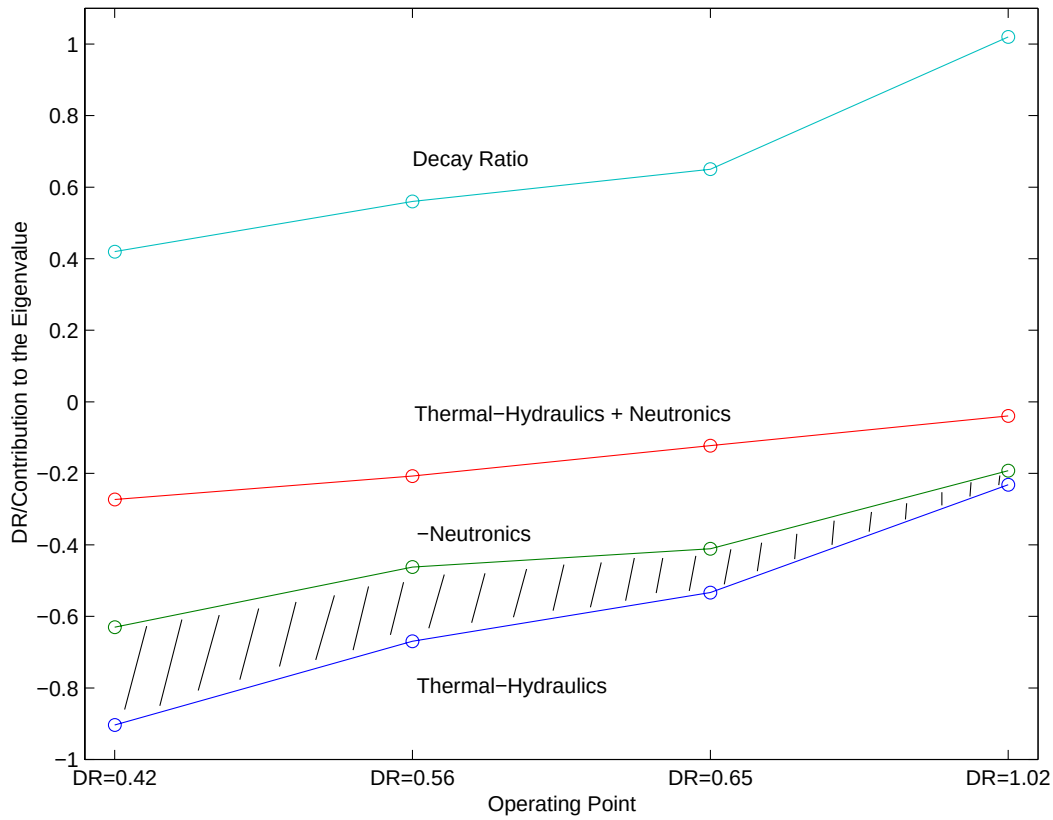

Figure 5.7: Comparison Between the Decay Ratio and the Contributions of the Reactor Core

5.4.2 Contribution of the Fuel Assemblies to the Eigenvalue during an Approach to Instability

In addition to the analysis of the contributions of different model sections, it is also interesting to investigate the contributions to the eigenvalue of the different fuel assemblies in the core. This is done in this section by examining a series of operating points in order of decreasing stability.

Figure 5.8 shows the power density of the Leibstadt reactor for a very stable operating point (DR ≈ 0.1). The corresponding plot with the contribution to the real part of the eigenvalue of the different fuel assemblies is shown in Figure 5.9. The colors represent the axially averaged value in each channel. Note that the sum of all channel values (times 25 nodes) added to the values in each node outside of the core, equal the real part of the eigenvalue of the dominating mode. Negative values have a stabilizing influence, whereas positive values have a destabilizing influence.

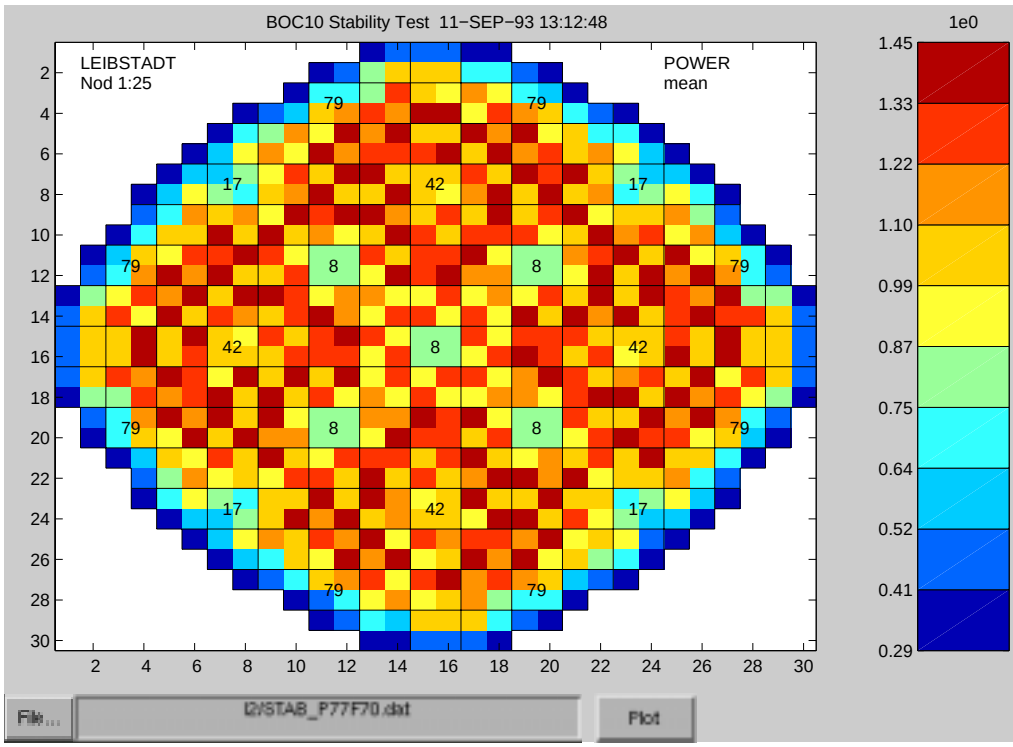

Figure 5.8: Power-Density Distribution for 77% Power and 70% Core Flow in Leibstadt

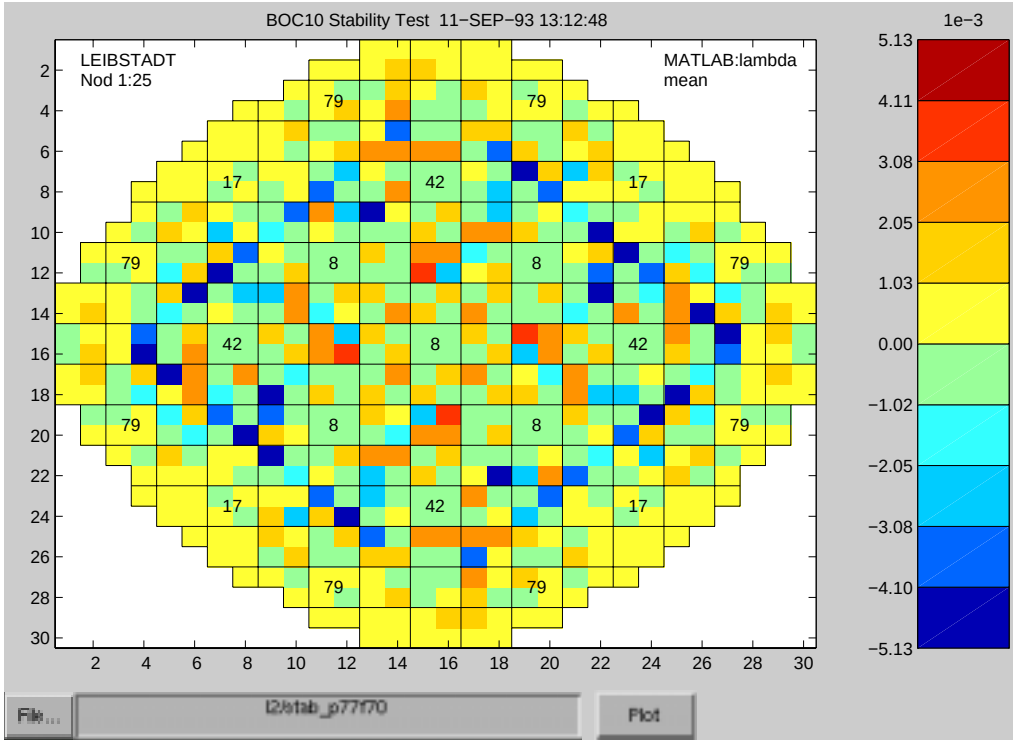

Figure 5.9: Contribution of Each Channel to the Eigenvalue for 77% Power and 70% Core Flow in Leibstadt

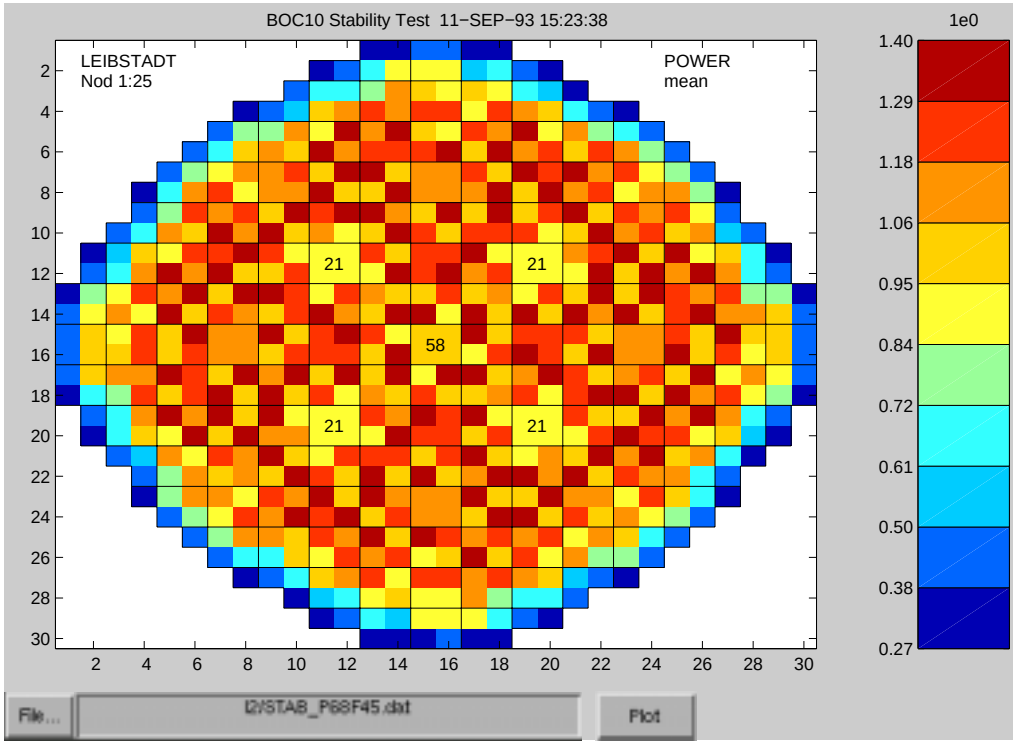

Figure 5.10: Power-Density Distribution for 68% Power and 45% Core Flow in Leibstadt

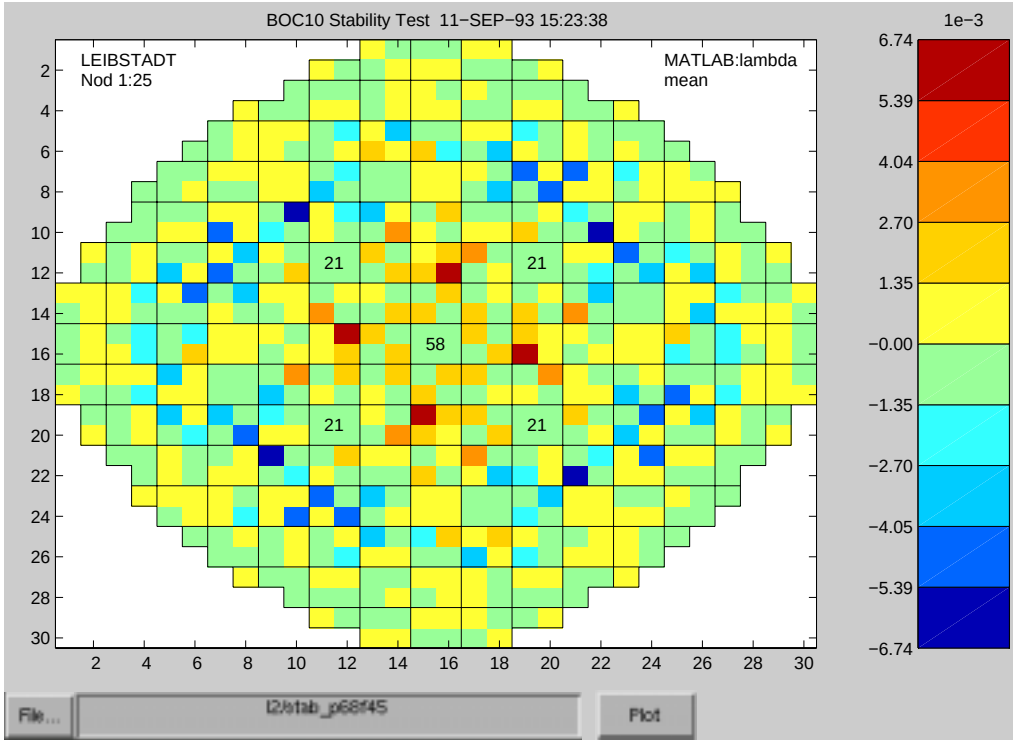

Figure 5.11: Contribution of Each Channel to the Eigenvalue for 68% Power and 45% Core Flow in Leibstadt

While the outer ring of fuel assemblies in the core are more or less neutral (low leakage strategy and ,therefore, low power density), there exists a ring of high-power-density assemblies with a large stabilizing effect (dark blue). These are the assemblies with a relative flat power density distribution. The strongly bottom-peaked assemblies with a high power density in the center of the core are destabilizing but largely outnumbered. As a result, the core is very stable.

The Figures 5.10 and 5.11 show the same information (power density, contribution to the real part of the eigenvector respectively) for the next operating point in the Leibstadt measurement series from 1993. The operating point is a bit less stable (DR ≈ 0.42) and it may be observed, that the radial distribution of the eigenvalue contributions became flatter. The above mentioned ring of stabilizing assemblies breaks up, and the destabilizing assemblies are found closer to the center of the core. The assemblies at the border of the core remain close to zero but move from a slightly destabilizing tendency to a slightly stabilizing tendency.

Figures 5.12 and 5.13 represent the next operating point (DR ≈ 0.56) in the measurement series. The break up of the “stabilizing ring” advances further, but the destabilizing assemblies in the center become less distinct. However, the latter effect is overshadowed by the former, since overall, the reactor is less stable. The contributions from the model section outside the core, remained roughly the same, as may be checked in Figure 5.6.

Figures 5.14 and 5.15 represent again the next operating point (DR ≈ 0.65) in the measurement series. The tendency is the same as in the figures before, with the exception, that the destabilizing assemblies in the center decreased in number but not in scale of the contribution.

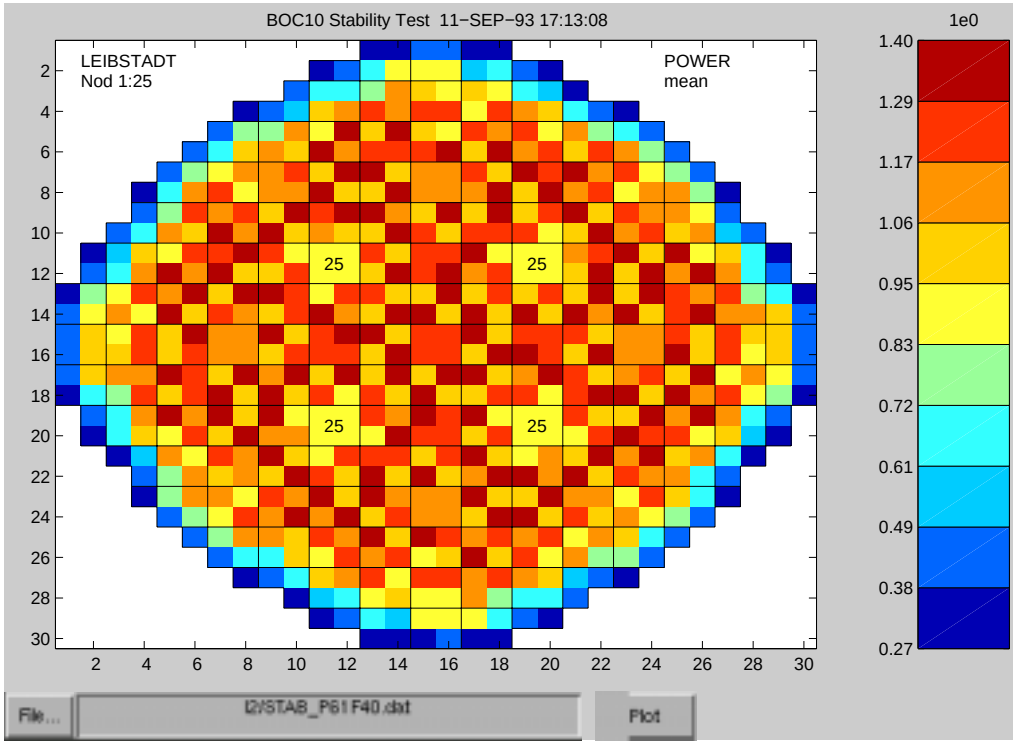

Figure 5.12: Power-Density Distribution for 61% Power and 40% Core Flow in Leibstadt

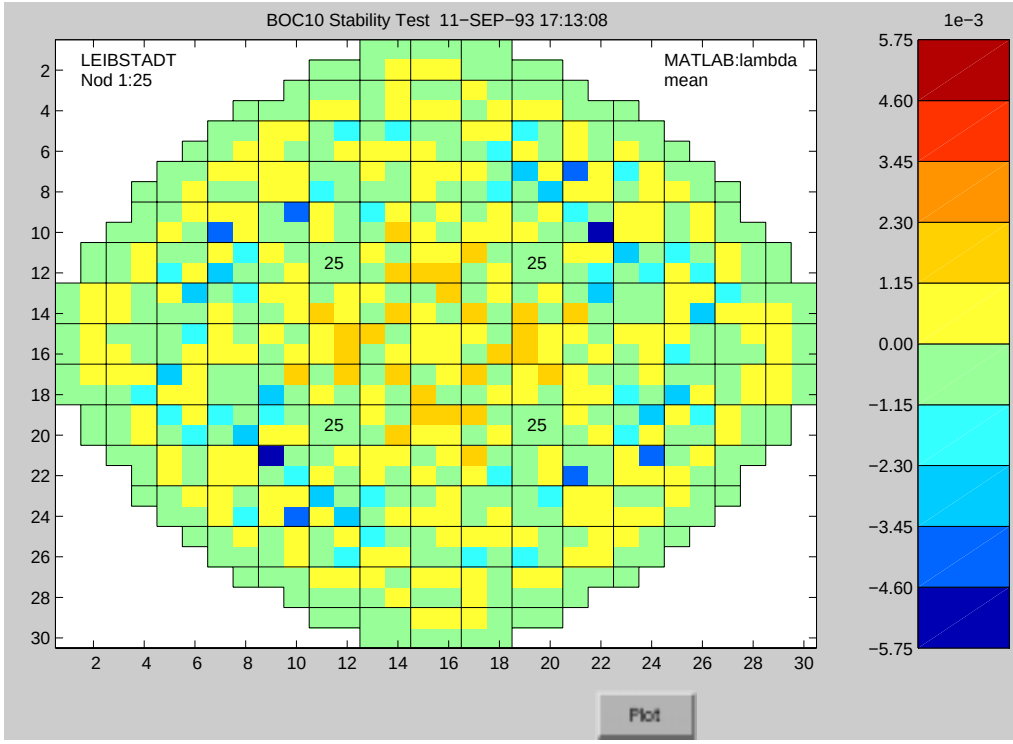

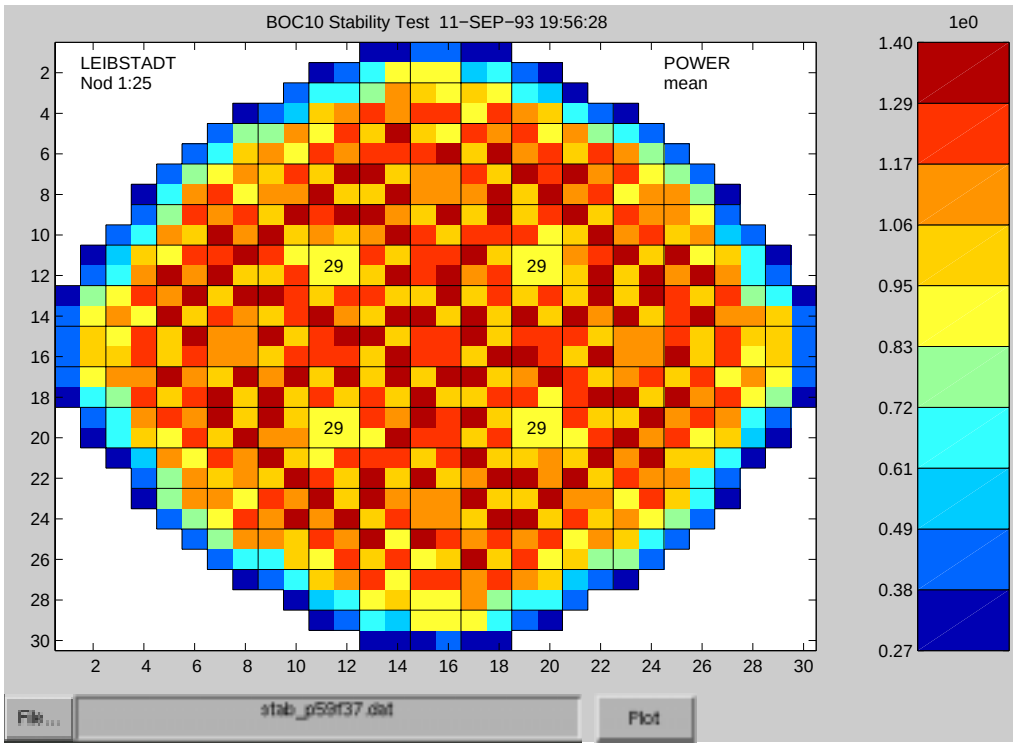

Figure 5.14: Power-Density Distribution for 59% Power and 37% Core Flow in Leibstadt

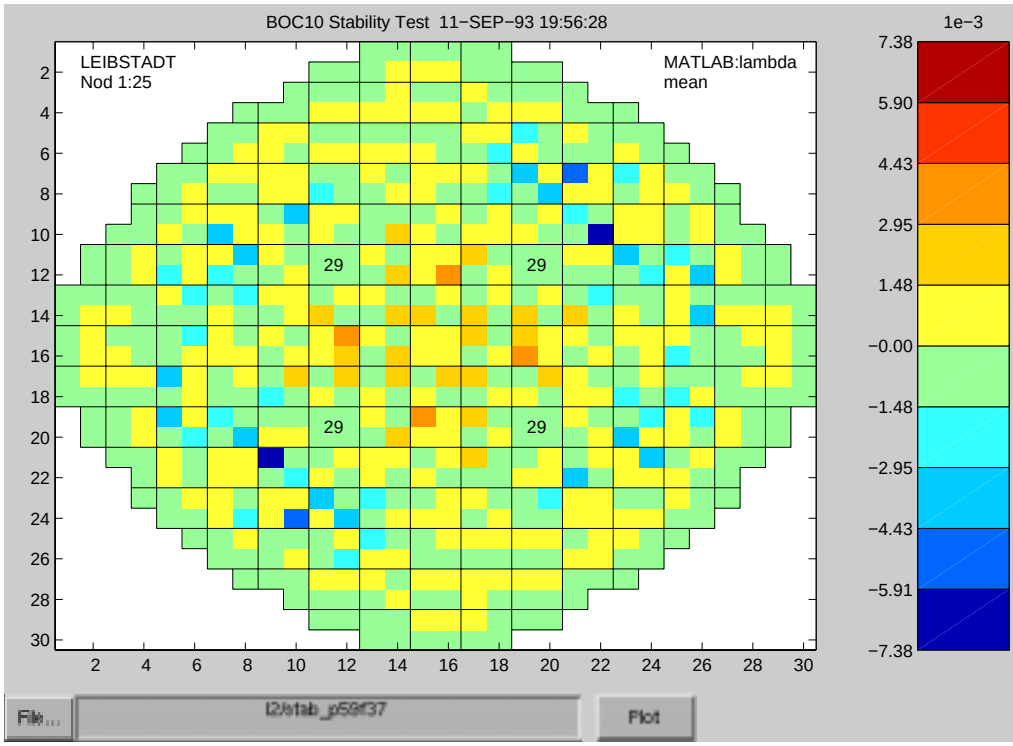

Figure 5.15: Contribution of Each Channel to the Eigenvalue for 59% Power and 37% Core Flow in Leibstadt

5.4.3 The Core of an Unstable Operating Point

Finally, Figures 5.16 and 5.17 show an unstable operating point (DR $\approx$ 1.0). The new aspect is, that the destabilizing center vanished completely, but two point-symmetric areas with a destabilizing effect appeared (orange). The radial shape of the distributions became reasonably flat with the exception of the two stabilizing areas (dark blue). It needs not much fantasy, to imagine a half core oscillation with the symmetry line from top left to bottom right, or from bottom left to top right. Even so, no regional oscillations were observed, this is in agreement with the high decay ratios for regional oscillations predicted by MATSTAB for the very same measurement series (see Table 6.6 on page 120).

One more interesting detail is that in contrast to the section-wise representation, in the assembly-wise representation not all contributions decrease (absolute value), the less stable an operating point is. The contribution of some fuel assemblies actually grows. The most extreme fuel assemblies (dark blue) in Figure 5.17 have a very large negative (stabilizing) contribution to the eigenvalue. Nevertheless, these assemblies are at the place where the regional oscillations reach their maxima and minima.

Figure 5.18 shows the part of the right eigenvector that represents the neutron flux for the dominating (global) mode at unstable operating conditions. According to Equation 2.25, this is also the driving force behind the time development. The arrows in the plot represent the phase and amplitude of the oscillation for some selected nodes. The black arrows are calculated by MATSTAB whereas the white arrows are measured with the LPRMs (Local Power Range Monitor for neutron flux). A detailed description on how the black and white arrows are calculated may be found in Section 6.1.2. In this representation, the absolute values of phase and amplitude have no physical meaning, only relative values are of interest.

Figure 5.19 shows the same information for the first regional mode. The plot shows that the amplitudes close to the symmetry line and close to the border of the core are, as expected, very small. The white arrows represent again the same measurement information as in the figure above. However, the scaling is different. For these two pictures, the scaling is done in such a way, that the first calculated phasor looks exactly to the right.

Since the calculations for this case predict a similar decay ratio for the global as well as for the regional case, it may be assumed, that the measured phasors contain a substantial regional component. It would therefore be prudent to add the calculated contributions from the global and regional modes. A comparison of these compound phasors should give even better agreement with the measurement data which naturally contains the superposition of all modes. It would also be interesting to compare the difference in amplitude of the global and regional component. Unfortunately, this cannot be achieved in a simple way, because MATSTAB has no information on how to scale the vectors. The basic problem is, that the eigenvectors may be multiplied with any complex number, and still stay the same eigenvectors. If the initial condition of the modes were known, Equation 2.25 could have been used. However, this is not the case.

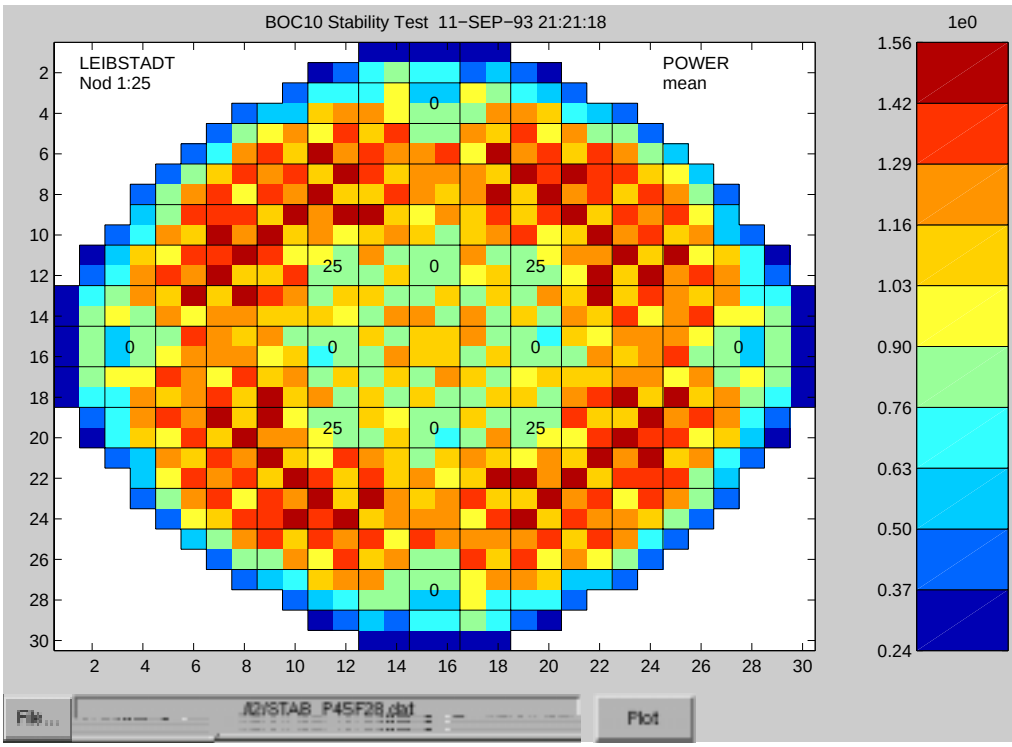

Figure 5.16: Power-Density Distribution for 45% Power and 28% Core Flow in Leibstadt, Reference Case

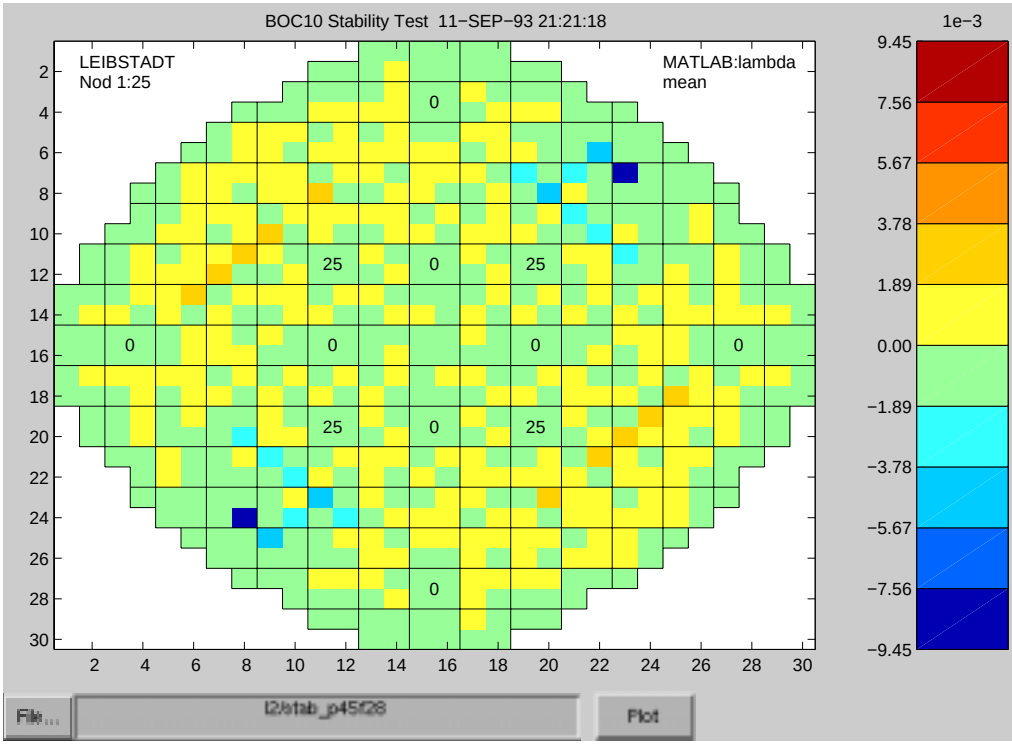

Figure 5.17: Contribution of Each Channel to the Eigenvalue for 45% Power and 28% Core Flow in Leibstadt, Reference Case

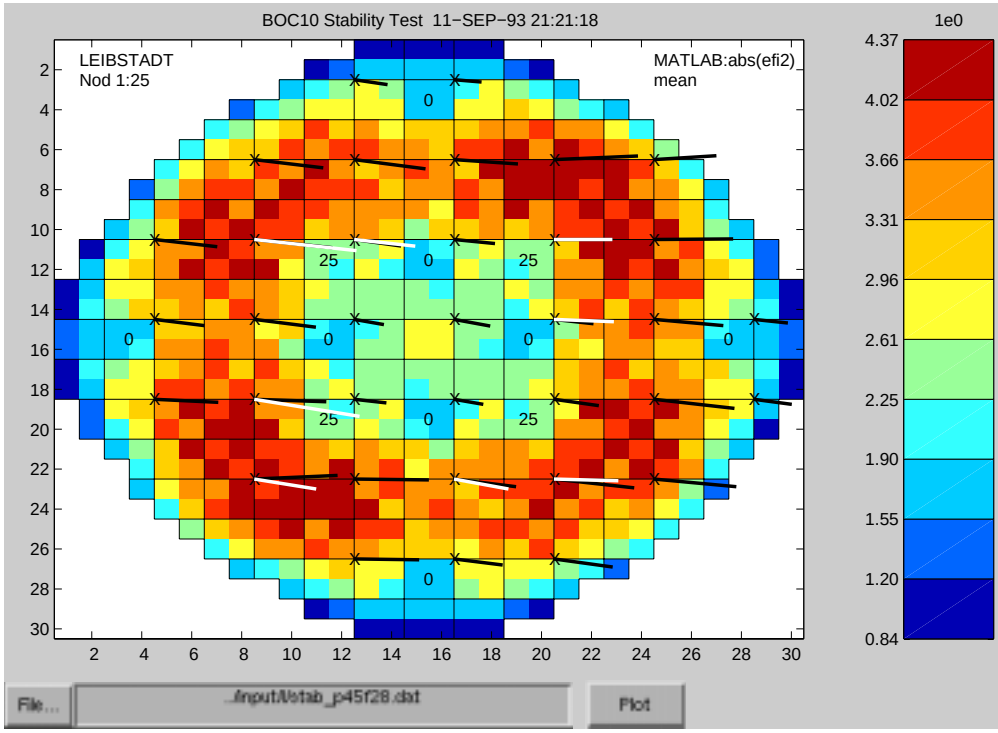

Figure 5.18: Comparison of MATSTAB and Measurement Point P45F28 in Leibstadt, Global Case

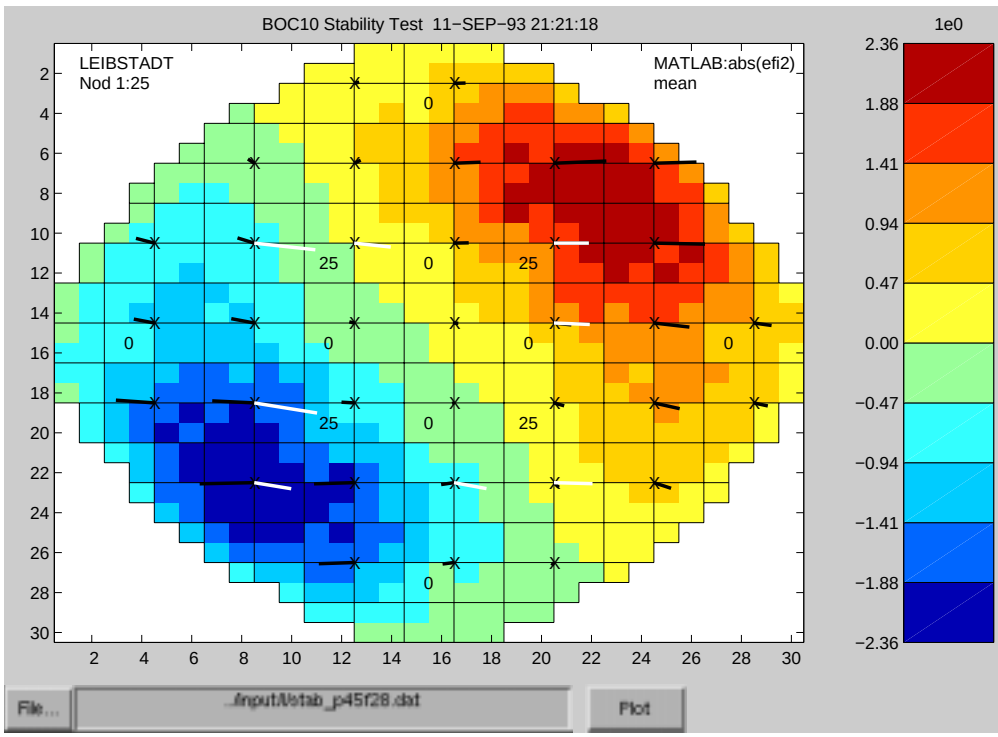

Figure 5.19: Comparison of MATSTAB and Measurement Point P45F28 in Leibstadt, Regional Case

In principle, the amplitudes could be approximately calculated if one does a least-squares fitting and solves the following equation set for C_1 and C_2.

$$C_1 * MATSTAB_{global} + C_2 * MATSTAB_{regional} = MEASUREMENT_{LPRM} \tag{5.21}$$

The uncertainty in the measurement itself, and the small number of LPRMs make this approach too unreliable to be of use.

A comparison between calculated and measured inlet flow data was done, but again the large uncertainty in the measurement data made a meaningful comparison impossible. For example, the relevant frequency of the oscillation could not be detected from Forsmark's inlet flow measurements.

5.4.4 Further Analysis Around an Unstable Operating Point

The Figures 5.20-5.25 show a brief analysis of the unstable operating point P45F28 shown in Figure 5.16 on page 74. While the reference case corresponds with an operating point measured in 1993 in Leibstadt, the other operating points are just a numerical investigation and were not realized with the reactor. All decay ratios and frequencies are listed in Table 5.1.

Case Description	DR Global	DR Regional	FR Global	FR Regional
Reference Case: Power 45% Core Flow 28%	1.02	1.03	0.42	0.45
Moderate Swap of the Control Rods	0.94	0.94	0.41	0.43
Extreme Swap of the Control Rods	1.23	0.78	0.44	0.43
Power Increase of 5%	1.13	1.18	0.42	0.45

Table 5.1: Investigation Around the Operating Point P45F28 with Power 45% and Core Flow 28% in Leibstadt

Figures 5.20 and 5.21 show the reactor after a moderate swap of control rods i. e. a moderate change in the power density distribution. The core power and the core flow were kept constant. One can observe that in comparison to the reference state (Figure 5.16) the extreme assemblies became fewer, but even more negative (down to -0.035 compared to -0.00945). Both the global and regional oscillation were stabilized, since in each quarter of the core, a control rod was inserted 25 percent. These control rods changed the radial power-shape just enough to make the core stable by a narrow margin.

Figures 5.22 and 5.23 show the reactor after a major swap of control rods. The rods are now inserted in the periphery rather than the center. The concentration of the high power assemblies in the center leads to a very unstable reactor (DR=1.23). The dominant fuel assemblies

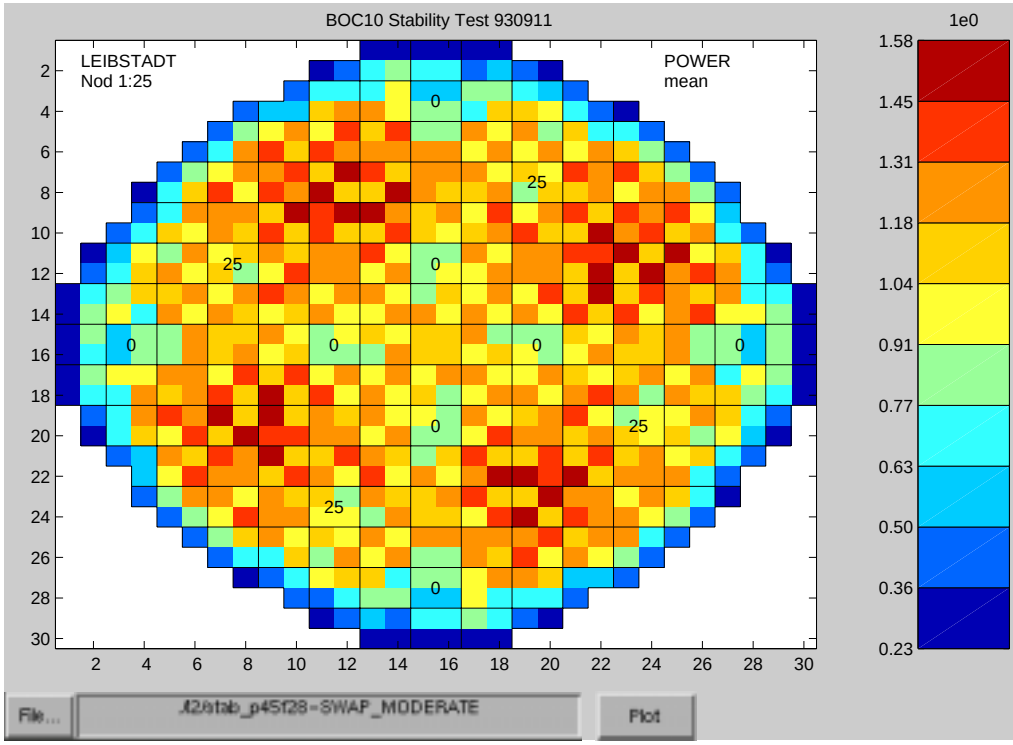

Figure 5.20: Power-Density Distribution After a Swap of Control Rods

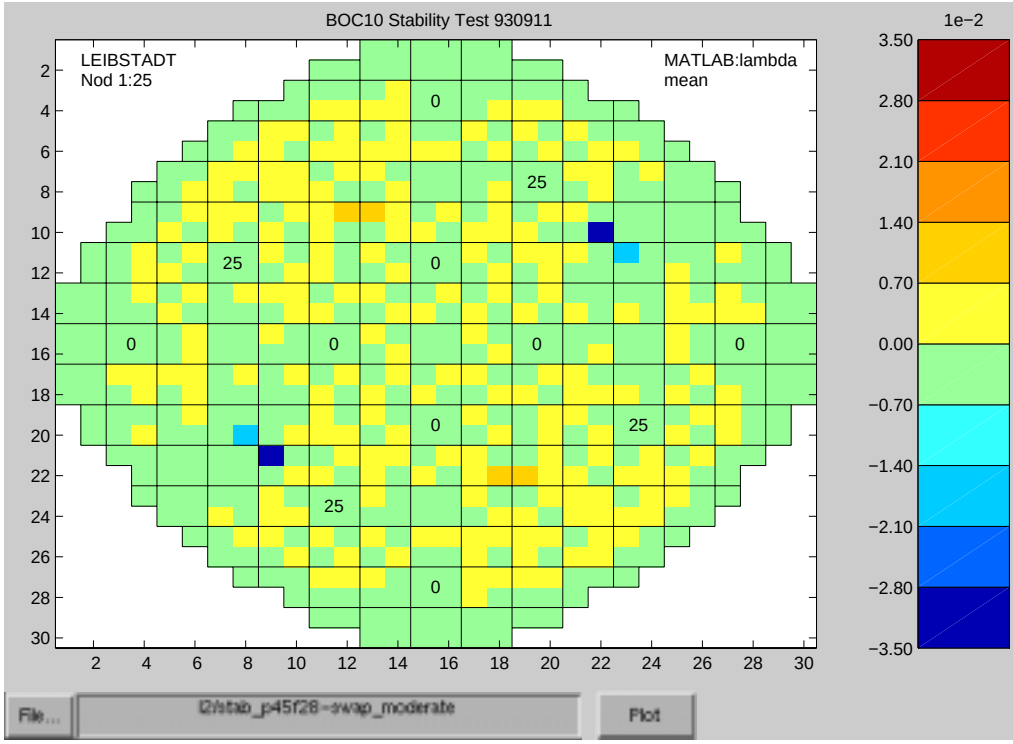

Figure 5.21: Contribution of Each Channel to the Eigenvalue After a Swap of Control Rods

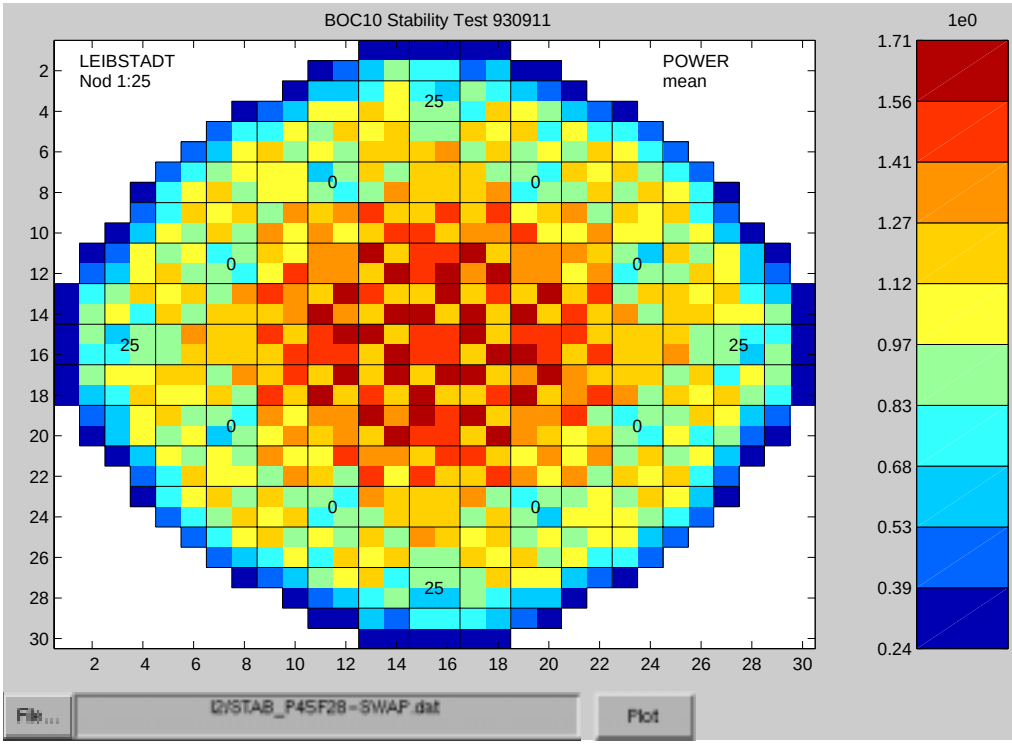

Figure 5.22: Power-Density Distribution After a Major Change in Control Rod Pattern

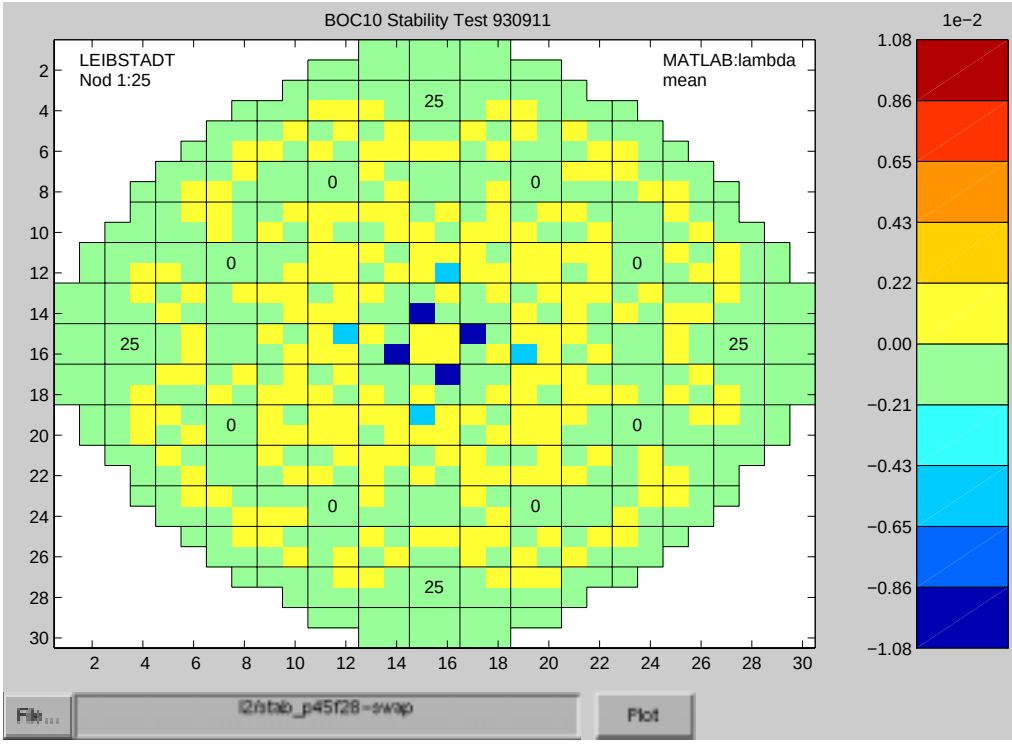

Figure 5.23: Contribution of Each Channel to the Eigenvalue After a Major Change in Control Rod Pattern

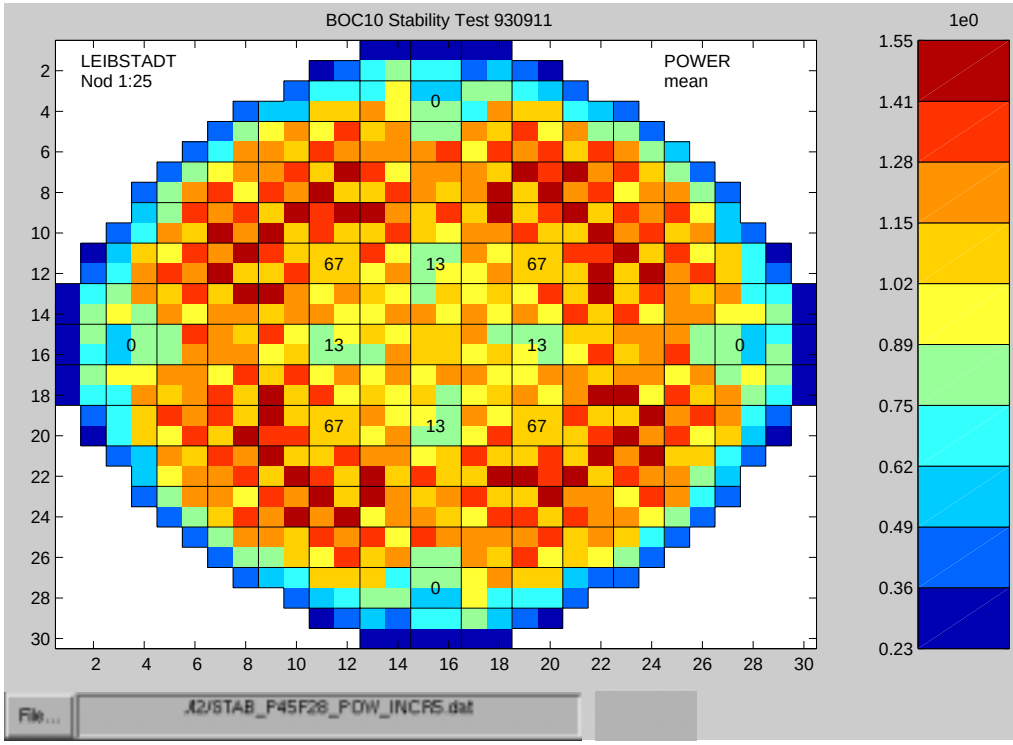

Figure 5.24: Power-Density Distribution After a Positive Change in Power

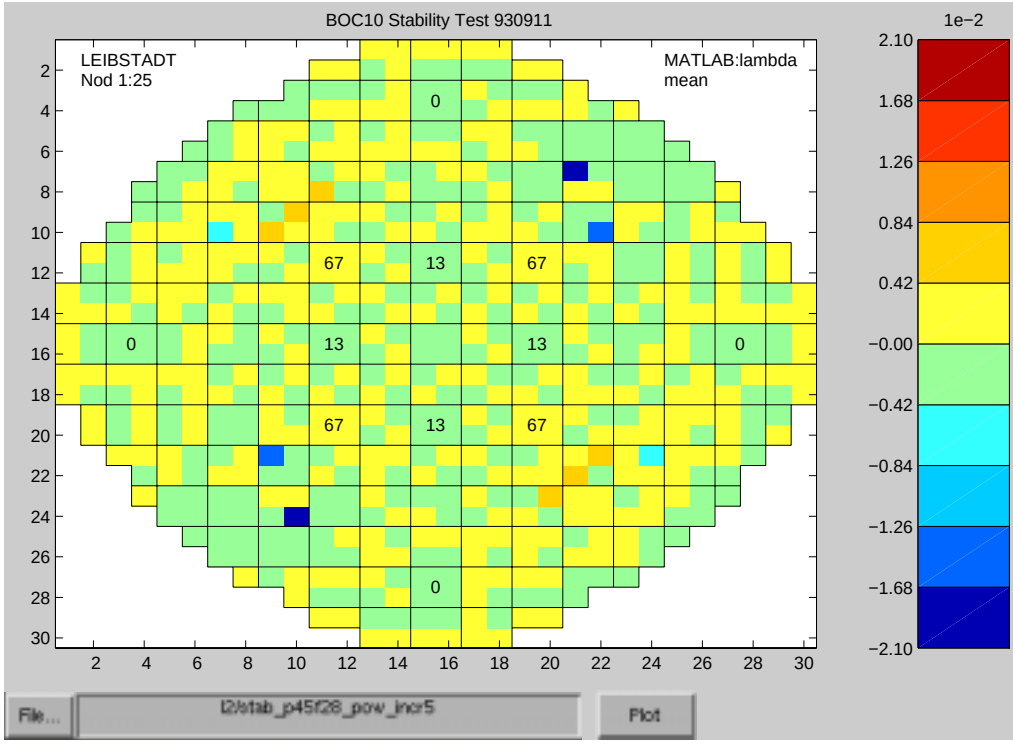

Figure 5.25: Contribution of Each Channel to the Eigenvalue After a Positive Change in Power

are larger in number, but smaller in their contribution (up to -0.0108 compared with -0.035 for the moderate swap). It is easy to spot that the high power density in the center of the reactor suppresses regional behavior, and that the global mode dominates. The numbers in Table 5.1 also give a clear verdict. DR global = 1.23 and DR regional = 0.78.

Figures 5.24 and 5.25 show the reactor after a power increase of five percent above the base case. Pulling the control rods while keeping the core flow constant, shifts the operating point of the reactor to a less favorable part of the power-flow map. Consequently, the decay ratio grew from 1.02 (reference case) to 1.13. In agreement with the measurement series shown in Figures 5.8-5.17, the stabilizing assemblies tend to become smaller in number but larger in scale for a less stable operating point.

Figures 5.26 and 5.27 show a comparison of the axial distribution of the eigenvalue contributions for the stable operating point (Figure 5.8) and the unstable reference case (Figure 5.16), respectively. The interesting information is that the first few nodes from the bottom normally give a positive contribution regardless whether the overall contribution of the fuel assemblies is positive or negative. This is expected, since the boiling boundary is around node four or five.

Figures 5.28 and 5.29 show the contribution to the eigenvalue from the same four fuel assemblies for the two operating points and confirm this observation. The four assemblies are chosen to be extreme cases in both plots. The location (coordinates) of the assemblies is plotted on the left side of the figures.

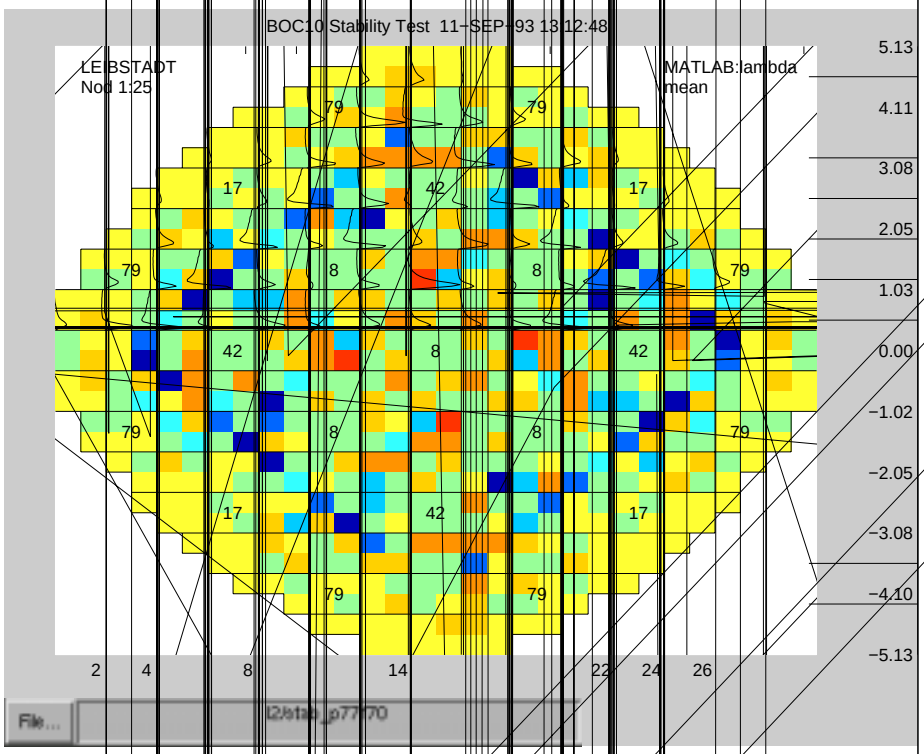
BOC10 Stability Test 11−SEP−93 13:12:48
LEIBSTADT
Nod 1:25
MATLAB:lambda
mean
5.13
4.11
3.08
2.05
1.03
0.00
−1.02
−2.05
−3.08
−4.10
−5.13
79
17
42
8
2
4
8
14
22
24
26
File...

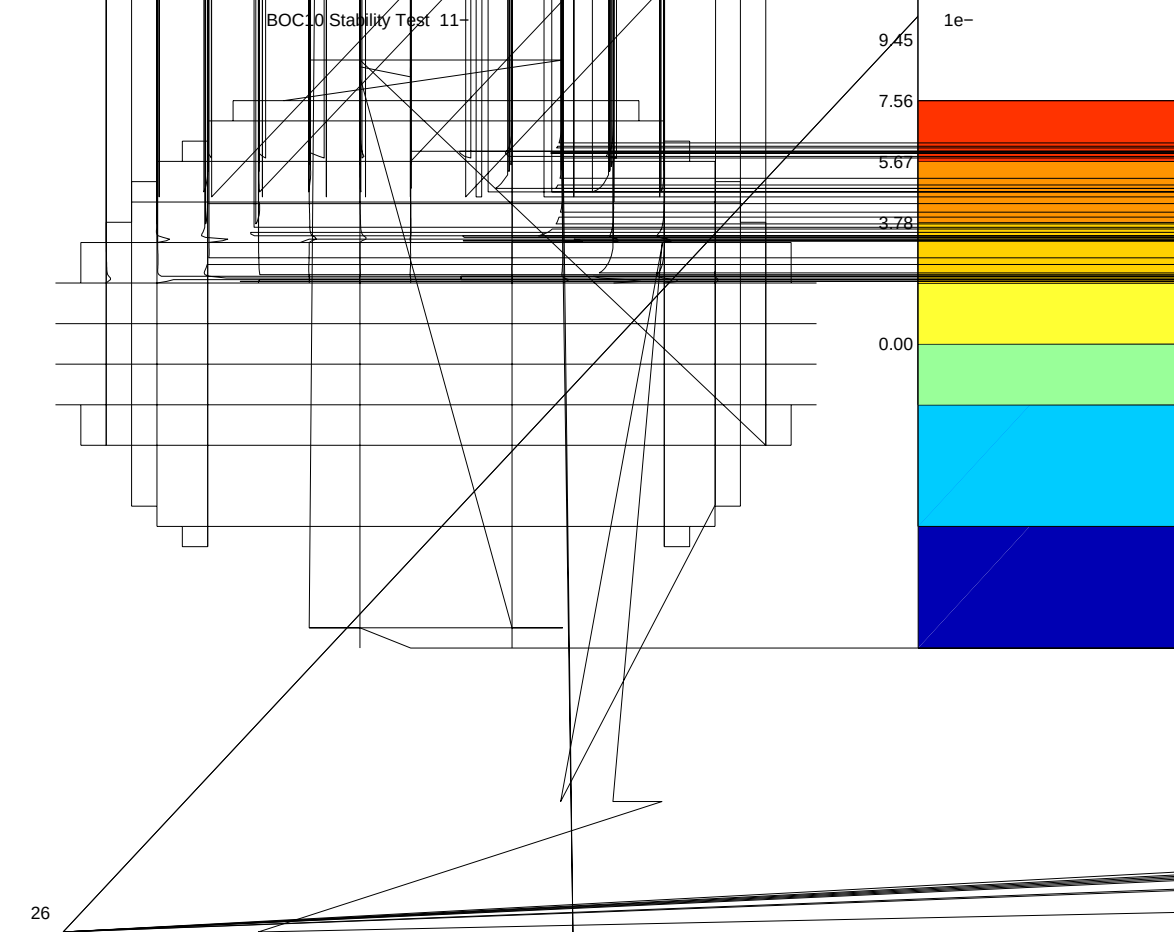
BOC10 Stability Test 11−
1e−
9.45
7.56
5.67
3.78
0.00

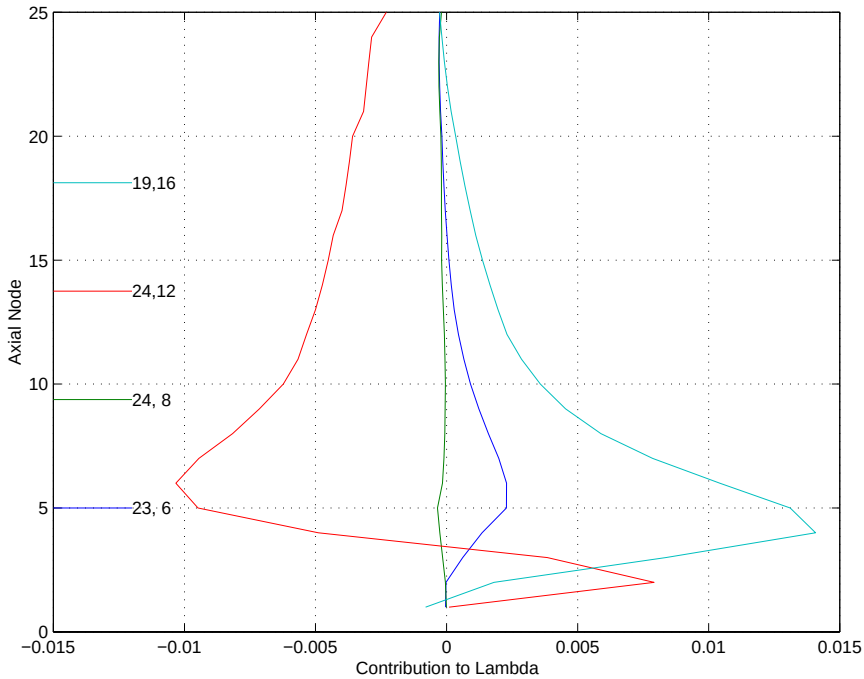

Figure 5.28: Axial Distribution of Contributions to the Eigenvalue for Extreme and Average Fuel Assemblies, Stable Case

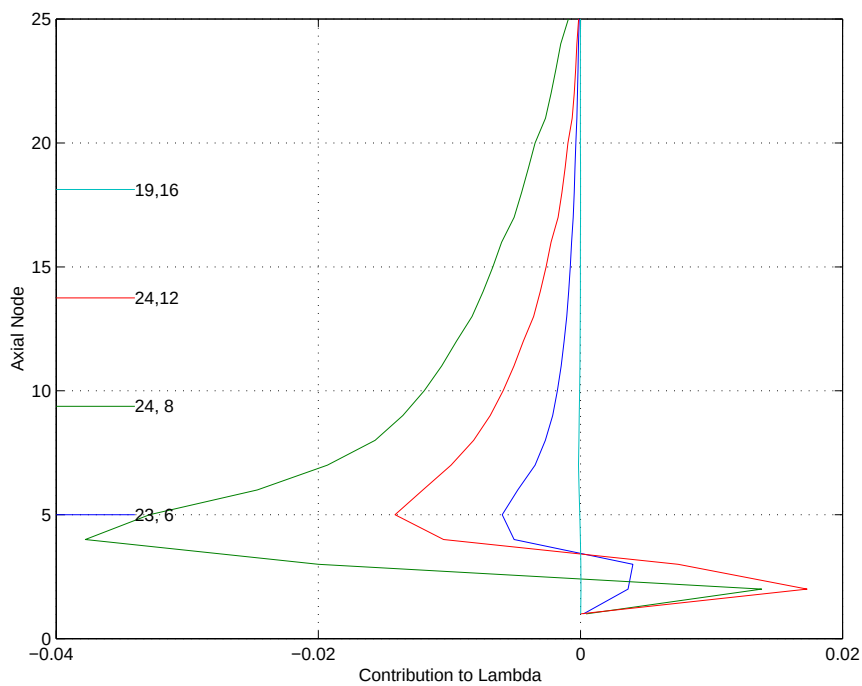

Figure 5.29: Axial Distribution of Contributions to the Eigenvalue for Extreme and Average Fuel Assemblies, Unstable Case

5.4.5 Contribution of Selected Equations and Variables to the Eigenvalue

Taking the level analysis one step further, it is possible to show for each equation or variable its contribution to the real part of the eigenvalue. The difference between the equation-wise and the variable-wise representation is, that in the former case, the rows of the matrix $\mathbf{A}_\lambda$ (Equation 5.7) are summed up, and in the latter case, the columns are summed up.

For example, the contribution of the void fraction equation shows how the void fraction gets affected by the other variables. Figure 5.30 shows, how much the void fraction equation in contributes to the real part of the eigenvalue.

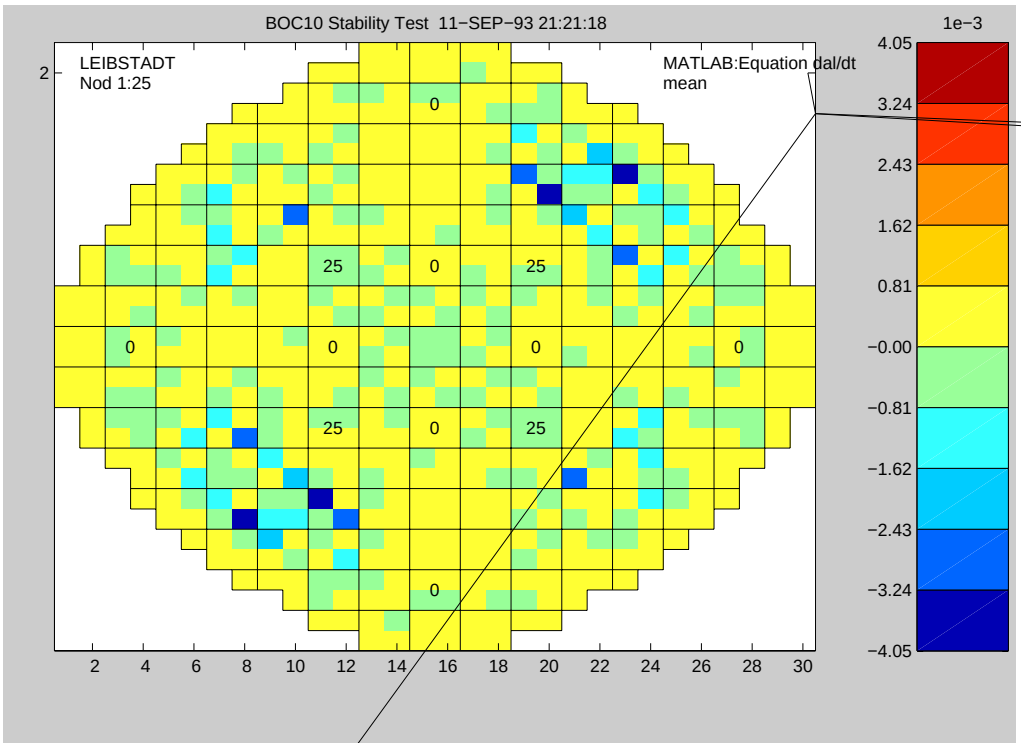

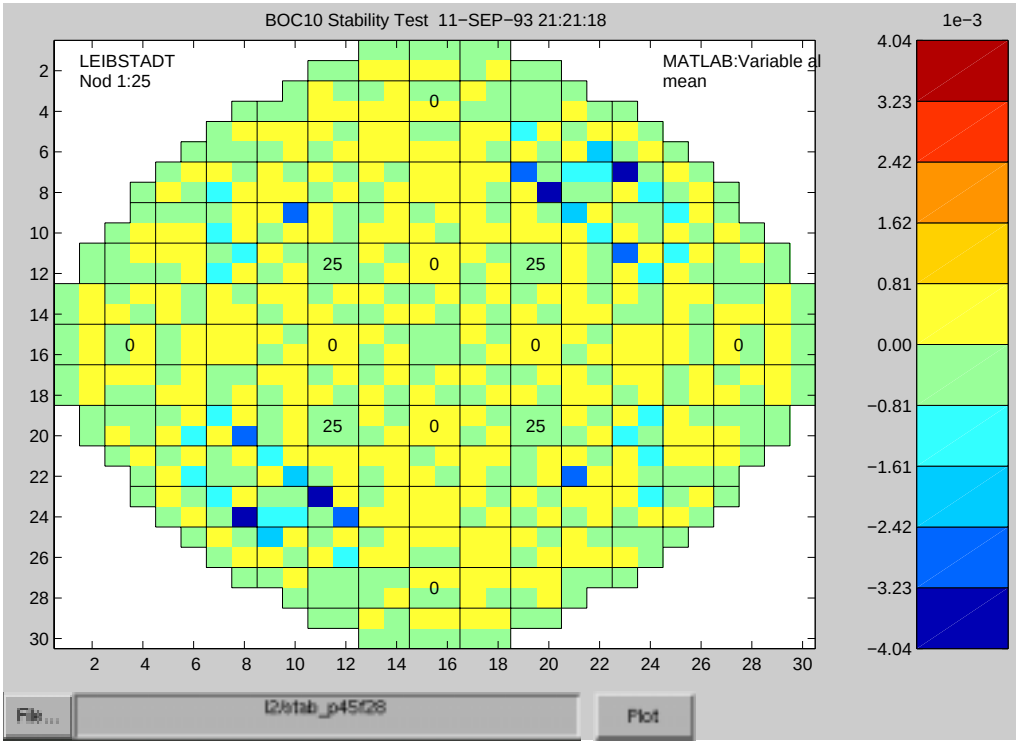

Figure 5.31: Contribution of the Variable Void Fraction to the Eigenvalue

contribution of other equations. This would actually imply, that the information present in these equations is not needed in the model. Further investigations are necessary to support this conclusion.

5.4.6 Analysis of Operating Points based on Eigenvalue Contribution Plots

To overcome the difficulties in interpreting the many thousands of contributions to the real part of the eigenvalue, as encountered in the previous sections of this chapter, the matrix $\mathbf{A}_\lambda$ from Equation 5.7

$$\mathbf{A}_\lambda = \begin{bmatrix} f_1 a_{1,1} e_1 & \dots & f_1 a_{1,n} e_n \\ \vdots & f_k a_{k,l} e_l & \vdots \\ f_n a_{n,1} e_1 & \dots & f_n a_{n,n} e_n \end{bmatrix} \tag{5.22}$$

is examined a bit further. To start width, two MATSTAB calculations with nearly identical operating points are compared. The only difference between the two calculations, is the pressure drop in the riser (input parameter VHO of MATSTAB). The reference calculation is the Leibstadt case presented in Figure 5.14 where the pressure drop over the riser is set to its default value (VHO=-7.0). The resulting decay ratio is 0.6475. The second case is exactly the same, but VHO=-20.0 and the resulting decay ratio is 0.6397.

Figure 5.32 shows the contribution of all equations in all nodes to the real part of the eigenvalue. The x-axis represents the equation number, and the y-axis represents the contribution to the eigenvalue. The ordering of the equations is the same as in the matrix $\mathbf{A}_\lambda$. A detailed description can be found in Table B.4 on page 161. The total number of equations is around 200'000. Since the difference in the two cases is very small, the red and the blue line in the plot can only be distinguished at a few places.

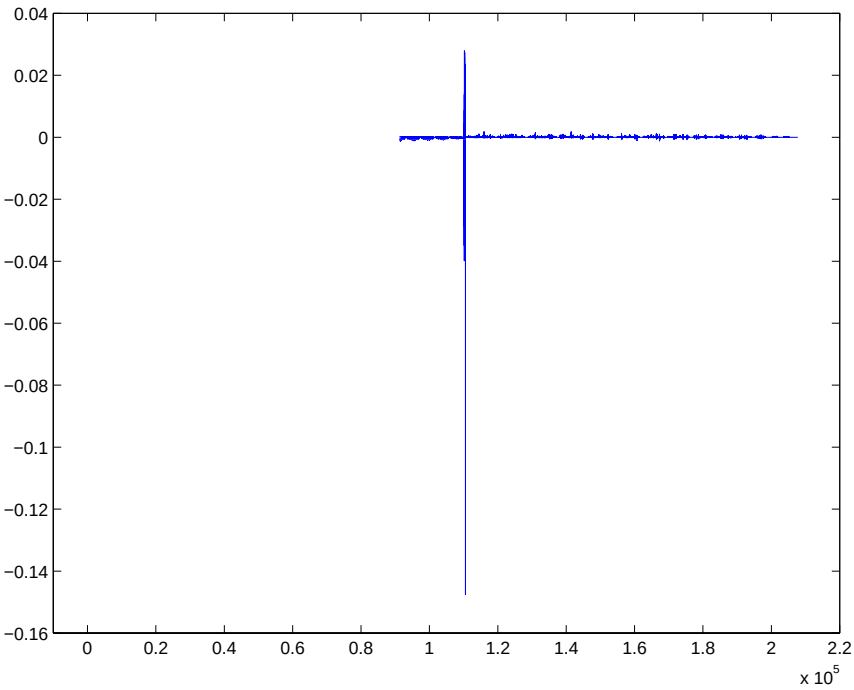

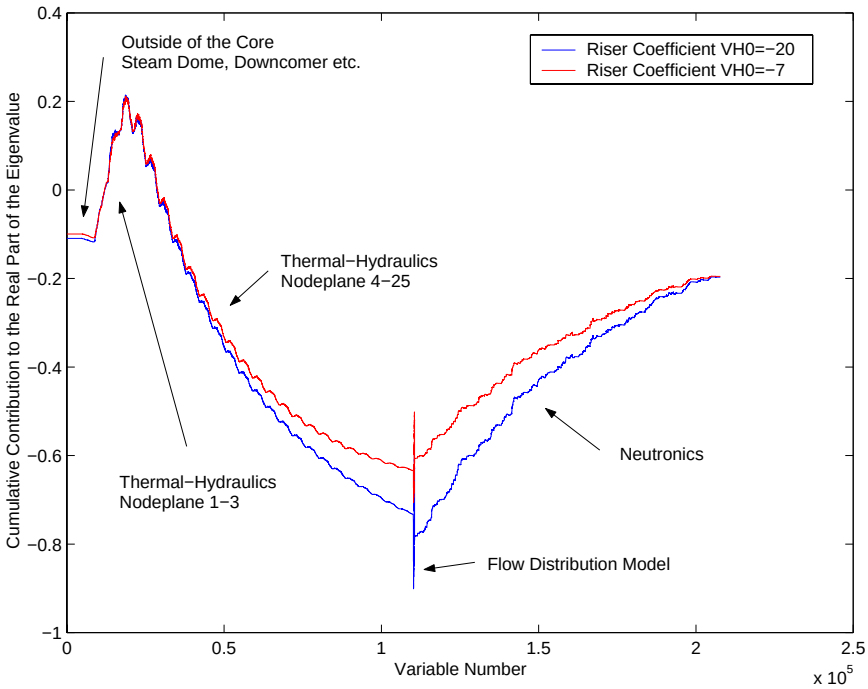

Figure 5.33: Cumulative Contribution: Equations

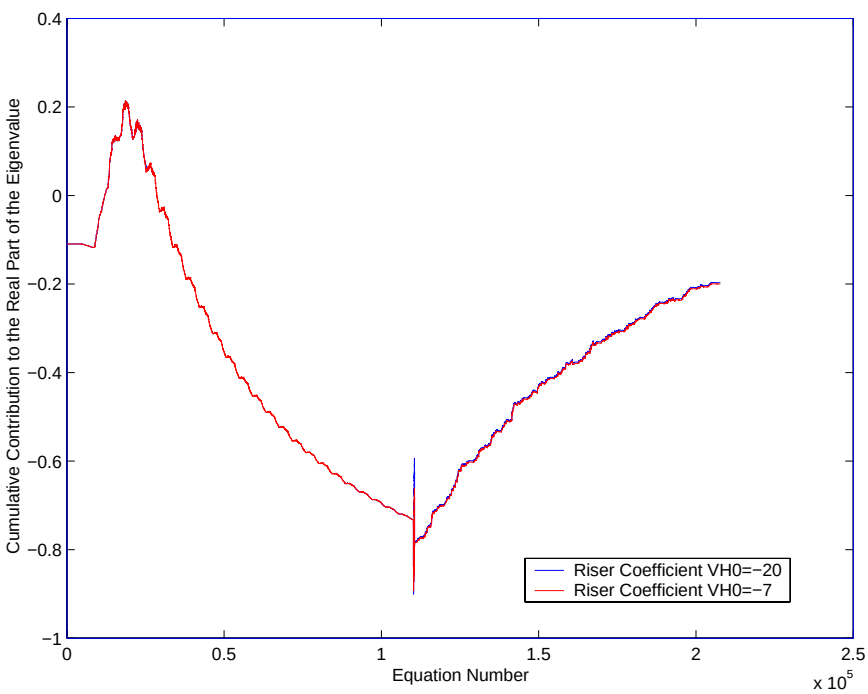

Figure 5.34: Cumulative Contribution: Equations (Using the Same Eigenvector)

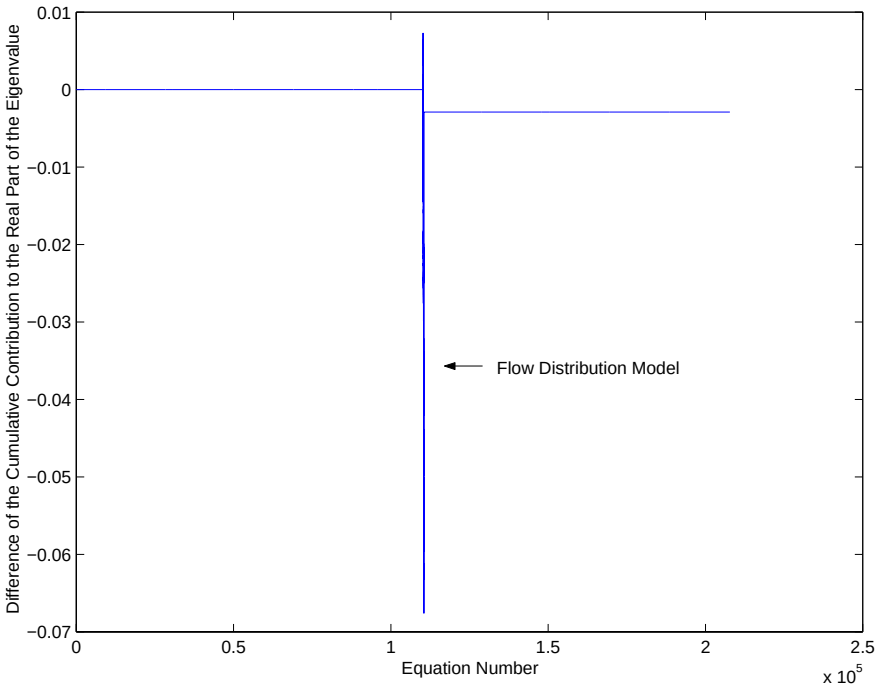

Figure 5.35: Difference of the Cumulative Contribution: Equations

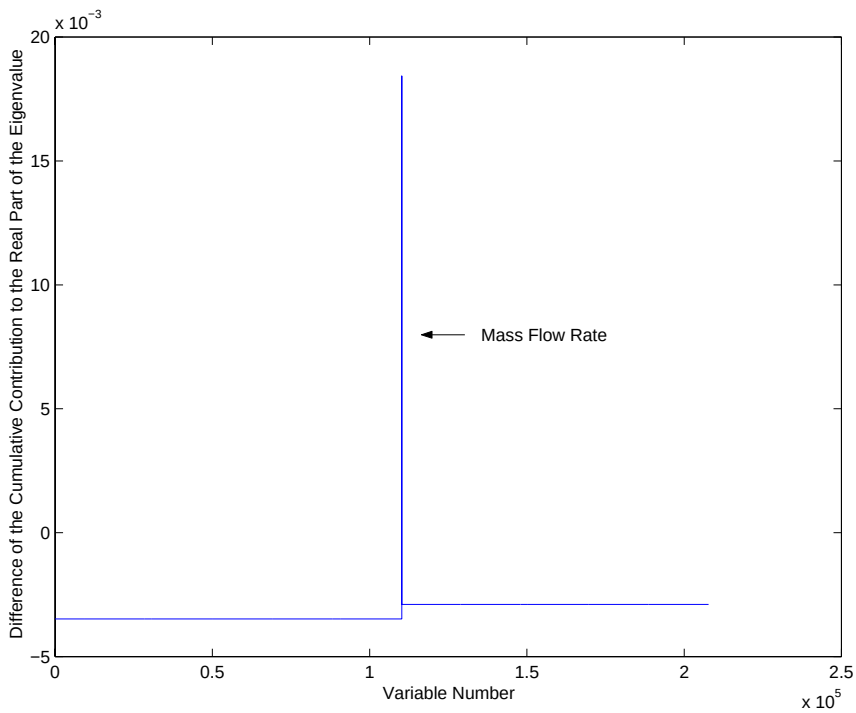

Figure 5.36: Difference of the Cumulative Contribution: Variables

the neutronics (larger positive contribution of the blue line in the second half of the plot). All together, both graphs end with a very similar eigenvalue.

A good impression of the real differences between the two cases can be achieved, if the eigenvectors from one of the two cases is used to calculate $\mathbf{A}_{\lambda}^{VHO=-7}$ and $\mathbf{A}_{\lambda}^{VHO=-20}$. In this case, the difference between the eigenvectors is neglected, and only the difference between the matrices is analyzed. The result is shown in Figure 5.34. The read and the blue graphs are now so close, that only a plot which shows the difference of the graphs may give more information. Figures 5.35 and 5.36 hence show the difference of the red and the blue graph in Figure 5.34. The plots confirm the observation that the two MATSTAB calculations differ mainly in the equations/variables around 110'000.

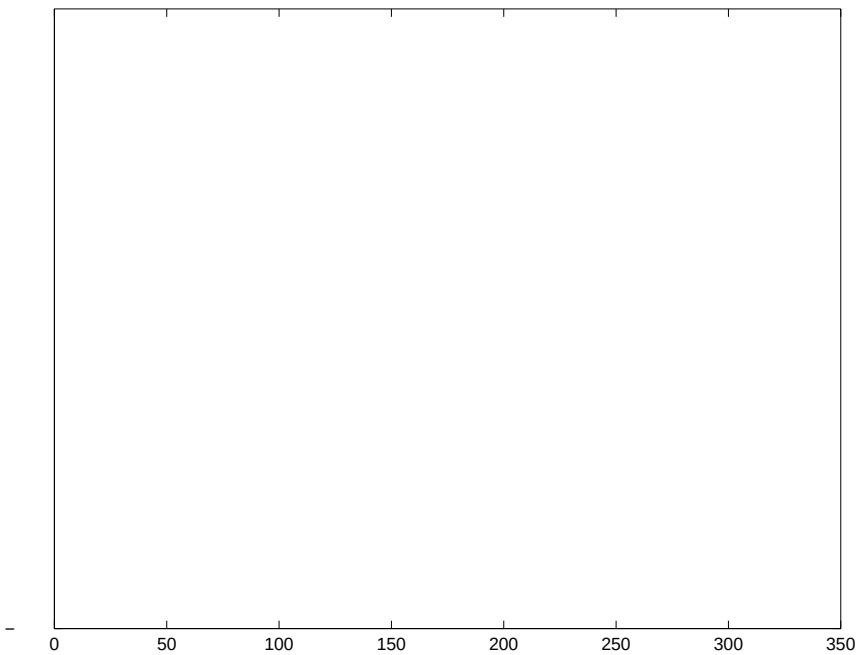

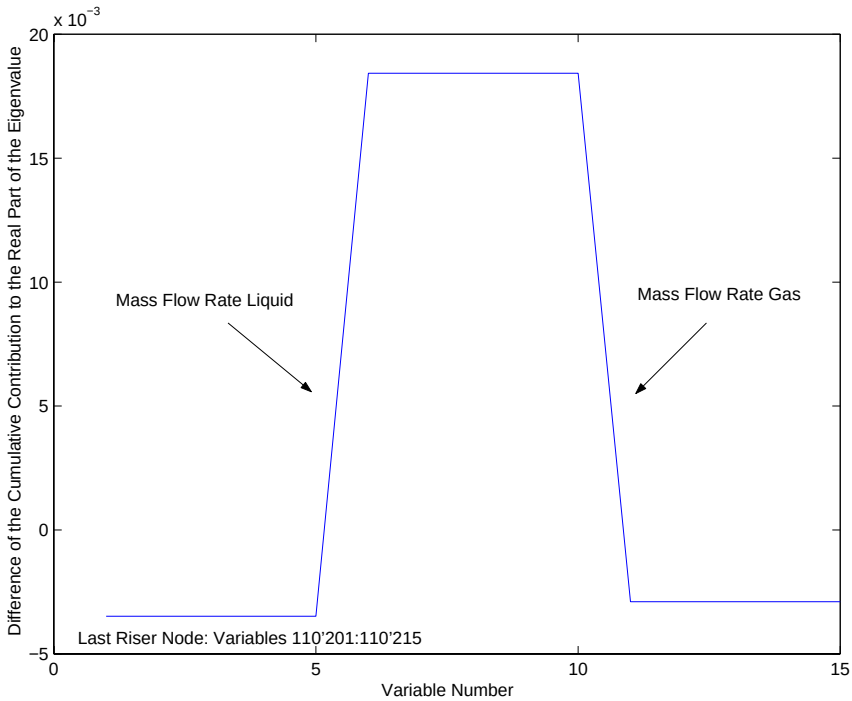

Figure 5.38: Difference of the Cumulative Contribution: Mass Flow Rate

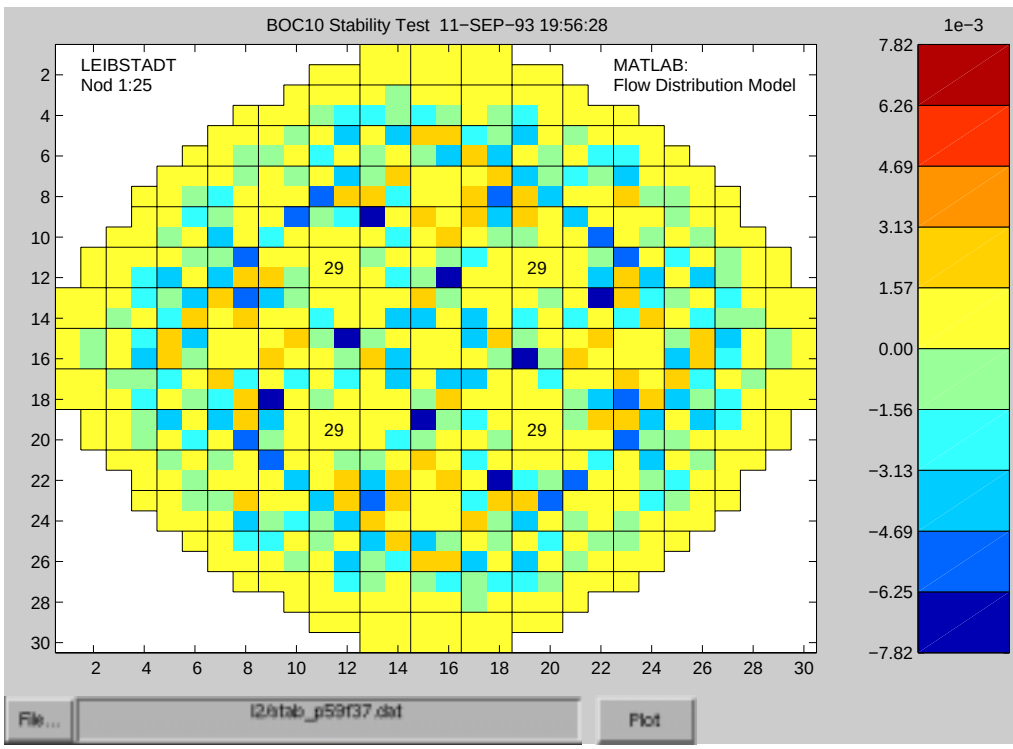

Figure 5.39: Difference of the Cumulative Contribution: Flow Distribution Model, Channel Wise

In concluding, it may be said, that the approach outlined above based on the cumulative contributions is an interesting new way to analyze the stability behavior of the reactor and pinpoints to sources of instability. The simple displays used identified correctly the sources causing changes in the eigenvalue/decay ratio and affecting stability.

5.4.7 Comparison of Different Operating Points in Leibstadt

Figure 5.40 shows the cumulative sums of the rows of the matrix $\mathbf{A}_\lambda$ for the Leibstadt measurement series from 1993. It can be seen very clearly that the stabilizing thermal-hydraulic contribution (left side of the plot) diminishes for a less stable operating point; the destabilizing contribution of the neutronics (right side of the plot) also diminishes. However, the overall effect is destabilizing since the reduction of the stabilizing thermal-hydraulics is larger. This observation is identical with the conclusion drawn from Figure 5.6.

Figure 5.41 shows the similar plot for the measurement series conducted in 1990. The contribution of the thermal-hydraulics to the eigenvalue behaves relatively systematic. The more stable an operating point is, the more negative (stable) is the thermal-hydraulic contribution. A bit more complex is the contribution of the neutronic part. Some of the graphs are convex, while other graphs are concave. The explanation is, however, pretty simple. The shape of the graph changes with the power density distribution. The change of control rods in the numerical experiment changed also the power density distribution, and therefore the contributions of the different fuel assemblies. Since the ordering of the equations is connected with the location of an assembly in the core, shift from the contributions from the center to the periphery, also changes the shape of the graph.

Concluding may be said, that the methods outlined in this chapter give a new angle to the stability investigations. The results show good agreement with measurements and experiences and seem to be promising. The proof, that completely new insights may be gained is, however, still missing.

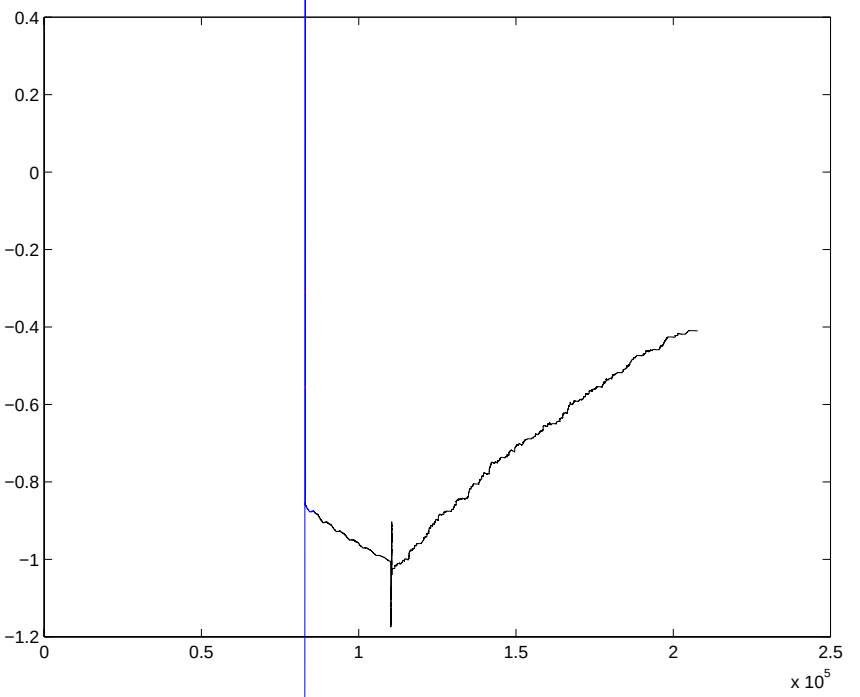
0.4
0.2
0
−0.2
−0.4
−0.6
−0.8
−1
−1.2
0
0.5
1
1.5
2
2.5
x 10^5

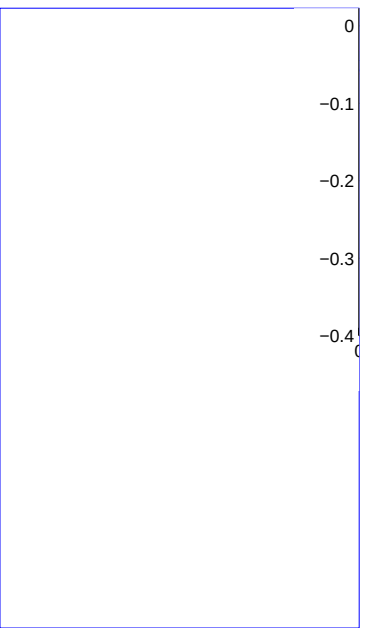
0
−0.1
−0.2
−0.3
−0.4

5.5 Sensitivity Analysis

Even though the decay ratio and the frequency of the oscillation are a direct and obvious description of the state of the reactor, the contained information is by far not complete. It is by no means obvious or true, why the connection between the decay ratio and a change in variable i.e. flow or power should be linear. Therefore, the decay ratio describes the stability of the investigated state, but does not give the distance (margin) to instability in a practical, "operational" manner.

One way to investigate the influence of a parameter p to stability is to evaluate many cases with slightly different values of p. This approach is normally limited by the computer time available. The MATSTAB model allows a much more efficient approach. The known eigenvalue $\lambda(p)$ is used to calculate the unknown eigenvalue $\lambda(p+\delta p)$.

Consider the matrix $\mathbf{A}$ with the eigenvalues $\lambda_1, \lambda_2, \ldots, \lambda_n$, right eigenvectors $\mathbf{e_1}, \mathbf{e_2}, \ldots, \mathbf{e_n}$ and left eigenvectors $\mathbf{f_1}, \mathbf{f_2}, \ldots, \mathbf{f_n}$ scaled in the way that $\mathbf{EF} = \mathbf{I}$.

Differentiation of the generalized eigenvalue Equation 2.15

$$\mathbf{A}\mathbf{e}_i = \lambda_i \mathbf{B}\mathbf{e}_i \tag{2.15}$$

with respect to any parameter p yields

$$\frac{\partial \mathbf{A}}{\partial p}\mathbf{e}_i + \mathbf{A}\frac{\partial \mathbf{e}_i}{\partial p} = \frac{\partial \lambda_i}{\partial p}\mathbf{B}\mathbf{e}_i + \lambda_i \mathbf{B}\frac{\partial \mathbf{e}_i}{\partial p} \tag{5.23}$$

Multiplying by $\mathbf{f_i^T}$ from the left

$$\mathbf{f}_i^T \frac{\partial \mathbf{A}}{\partial p}\mathbf{e}_i + \lambda_i \mathbf{f}_i^T \mathbf{B}\frac{\partial \mathbf{e}_i}{\partial p} = \frac{\partial \lambda_i}{\partial p}\mathbf{f}_i^T \mathbf{B}\mathbf{e}_i + \lambda_i \mathbf{f}_i^T \mathbf{B}\frac{\partial \mathbf{e}_i}{\partial p} \tag{5.24}$$

and solving for the derivative of the eigenvalue leads to the important relation

$$\frac{\partial \lambda_i}{\partial p} = \frac{\mathbf{f}_i^T \frac{\partial \mathbf{A}}{\partial p}\mathbf{e}_i}{\mathbf{f}_i^T \mathbf{B}\mathbf{e}_i} \tag{5.25}$$

From a calculated state with parameter p, the eigenvalue for the slightly different state with the parameter p+δp can be deduced as follows.

$$\lambda_i(p+\Delta p) = \lambda_i(p) + \left(\frac{\mathbf{f}_i^T(p)\frac{\partial \mathbf{A}(p)}{\partial p}\mathbf{e}_i(p)}{\mathbf{f}_i^T(p)\mathbf{B}\mathbf{e}_i(p)} \right) \cdot \Delta p \tag{5.26}$$

This result is useful, because the stability margin of the new state is obtained without calculating its eigenvalue from scratch. It is also one additional way to understand that the information about the stability behavior of the reactor is contained in the eigenvectors.

Example: Slip

One obvious application of Equation 5.26 would be for a small change in power. However, a change in power would also affect many other variables, e.g. the void fractions. Therefore, a new steady-state file from POLCA would be necessary and the effects of all other implied changes would be superimposed upon those of the initial power change.

The Bankoff-Malnes correlation

$$w_g = \mathrm{Sw_l} + \mathrm{w^0} \tag{A.95}$$

relates the vapor velocity w_g to the liquid velocity w_l, using a slip factor S. This factor is not expected to change in time. However, its value is not so easy to measure directly in a real NPP. Therefore the uncertainty in the slip is very often used to fit the power-shapes of the modeling code to the measured data.

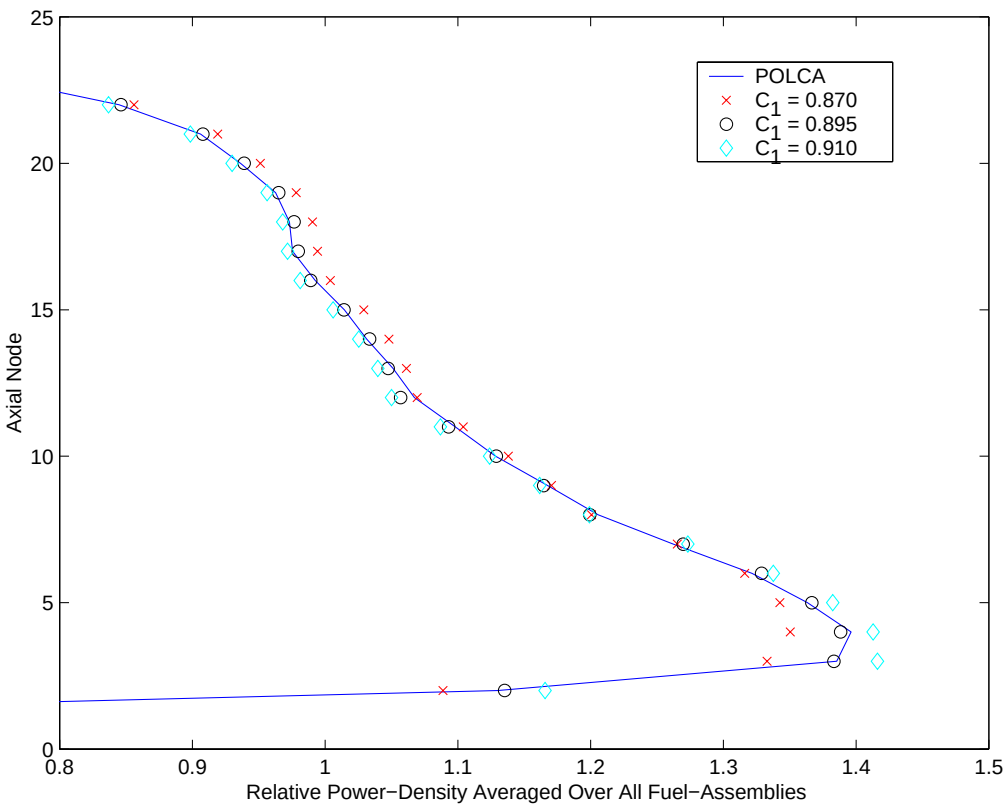

Figure 5.42: Influence of the Slip Parameter c_1 S to the Radially Averaged Power-Density Distribution

Figure 5.42 shows the radially averaged relative power-density distribution for the operating point considered (calculated by POLCA) compared to MATSTAB calculations using different values for c_1 in the slip correlation A.96.

$$S = \frac{1-\alpha}{c_1 - \alpha} \tag{A.96}$$

The influence of S (respectively c_1) can be seen as clearly as the rather optimal value of 0.895 which is used normally by MATSTAB.

Equation 5.26 is now used to study the effect of a change in S (c_1) on stability. The base of the investigation is the operating point with 59% power and 4010 kg/s core flow from the Leibstadt Cycle-ten measurement. The measured decay ratio was 0.65 and its frequency was 0.50. Table 5.2 shows the influence of the slip parameter S upon the decay ratio and frequency. All values from the sensitivity calculation were derived using $C_1 = 0.895$ as base and $\Delta C_1 = 0.005$ as deviation.

	Full Calculation		Sensitivity Anal.	
Slip (c_1)	DR	FR	DR	FR
0.885	0.6362	0.4321	0.6350	0.4323
0.890	0.6421	0.4340	0.6432	0.4339
0.895	0.6514	0.4356		
0.900	0.6599	0.4373	0.6596	0.4372
0.905	0.6695	0.4387	0.6679	0.4389
0.910	0.6742	0.4402	0.6762	0.4405

Table 5.2: Decay Ratio and Frequency for Different Slip Values

The predictions of the sensitivity analysis show good agreement and lie within the accuracy of the MATSTAB calculation itself. Even though this method is not usable for large steps, it is possible to make a very quick judgment on how the change of a parameter may influence the result.